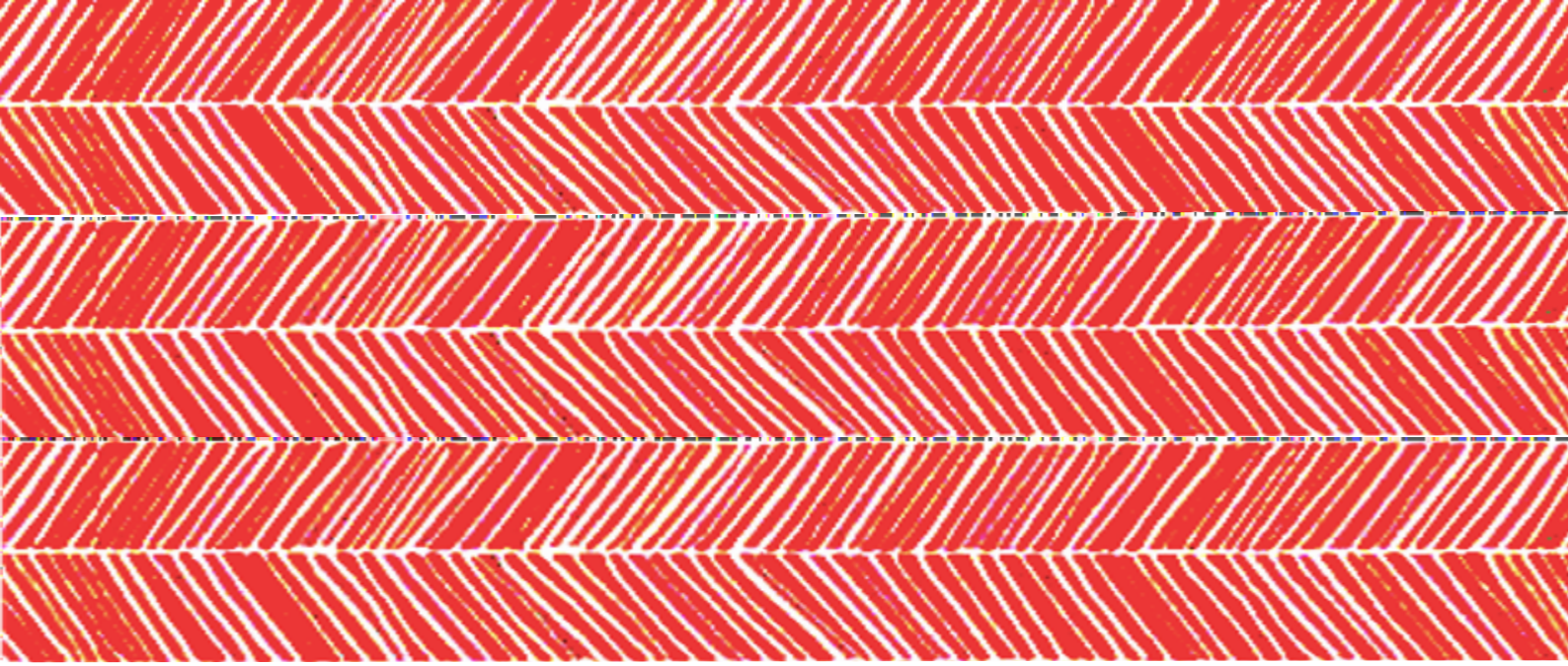

Using ultrasound muscle imaging to assess the proportionality between ankle angle and contractile element length

A feasibility study to test the assumption with plane-wave ultrasound and system identification of joint dynamics

B. W. Ossenkoppele

TU Delft

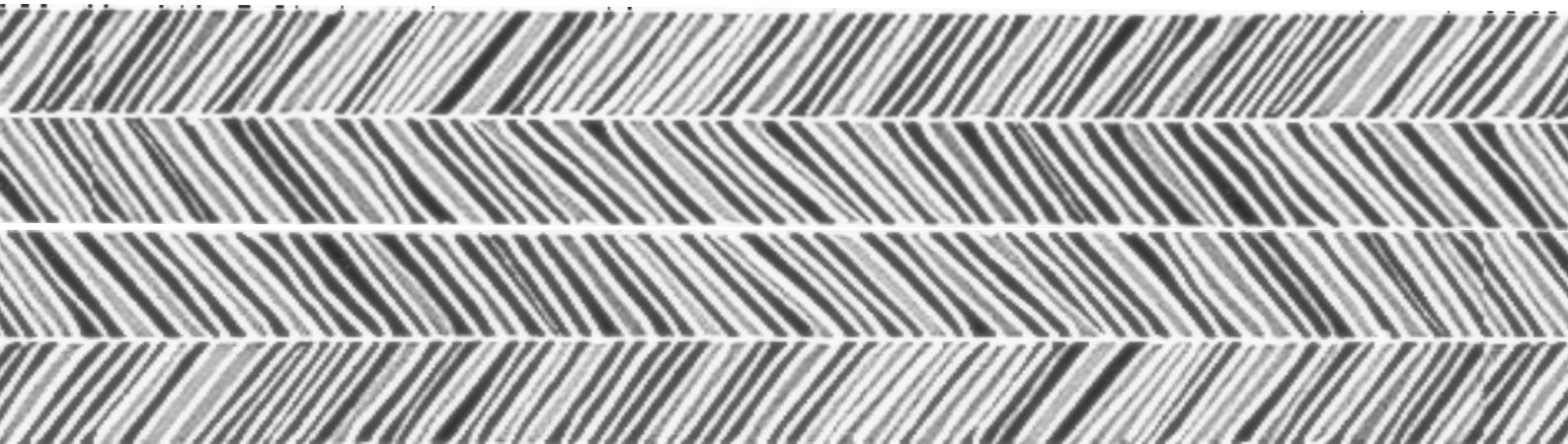

Using ultrasound muscle imaging to assess the proportionality between ankle angle and contractile element length

A feasibility study to test the assumption with plane-wave ultrasound and system identification of joint dynamics

by

B.W.Ossenkoppele

to obtain the degree of Master of Science
at the Delft University of Technology,
to be defended publicly on Friday April 20, 2018 at 15:00 AM.

Student number:	4077067	
Thesis committee:	Dr. ir. A. C. Schouten,	TU Delft
	Dr. ir. W. Mugge,	TU Delft
	Ir. K.E. Rodriguez Hernandez,	TU Delft
	Prof.dr. ir. N. de Jong,	TU Delft
	Dr. ir. V. Daeichin	TU Delft

An electronic version of this thesis is available at `http://repository.tudelft.nl/`.

TU Delft

Using ultrasound muscle imaging to assess the proportionality between ankle angle and contractile element length

A feasibility study to test the assumption with plane-wave ultrasound and system identification of joint dynamics

Boudewine Willemine Ossenkoppele

***Abstract*—Ultrasound gives the opportunity to look at muscles and observe their change in length. This tool has increased the knowledge about muscle-tendon dynamics and sometimes revealed surprising muscle stretch behaviour. System identification experiments use robots to disturb the ankle and measure its torque and angle. Muscle movement is derived from the measured joint angle and their assumed relationship. This study uses plane-wave ultrasound imaging to investigate the relation between ankle angle and muscle length during system identification experiments. The first goal is to determine the feasibility of using ultrasound measurements for system identification. The second goal is to investigate the validity of the assumption that muscle stretch is proportional to ankle angle and the effect of this assumption on the prediction of reflex size. Transient and continuous disturbances were applied to the ankle, while images of the soleus and gastrocnemius were recorded with ultrasound and processed with an image tracking algorithm. For small (1° SD) continuous perturbations ankle angle and muscle length can be assumed proportional during a relax task. However, a conclusion cannot be drawn for the position task due to the low coherence of the muscle length measurements. For transient perturbations with a high velocity ($> 90^\circ$/s) the muscle length showed oscillations that were not present in the ankle angle, demonstrating a non-proportional relationship. The gastrocnemius velocity predicted the size of the short latency reflex better than the perturbation velocity of the ankle robot. Using plane-wave ultrasound imaging for system identification experiments was feasible.**

***Index Terms*—ultrasound, plane-wave, ankle joint, system identification, muscle, proportional**

I. Introduction

WHEN we see someone making a movement we do not see all that is taking place inside the body to make this happen. The muscles create movement. Muscle fibres convert the electric signals from the central nervous system into a muscle contraction. The tension formed in the muscle fibres is transmitted via a tendon to the skeletal system where the force creates a moment on a joint. This moment can be needed to move the joint into a different configuration or it can be necessary to keep the limb in a constant position. Keeping our limbs in a constant posture is important in many daily situations, such as standing or driving a car on a bumpy road [1], [2].

To achieve posture control the body has to deal with unpredictable disturbances that change the posture [3]. Disturbances can be either short and sharp, such as a deep bump in an otherwise flat road or longer lasting. An example of the last could be the disturbances caused by driving over a gravel path. Both of these types of perturbations are used in the investigation of posture control. They are usually labelled as transient [4], [5] and continuous perturbations [3].

One instantaneous mechanism that can be used to counteract undesired effects of external perturbations is to co-activate the agonist and antagonist muscles (co-contraction) which increases the viscoelastic properties of the muscle [6]. The second fast mechanism available for resisting perturbations are reflexes originating from the sensory organs in the muscle and tendon: the muscle spindle (MS) and Golgi tendon organ (GTO) [7]. Reflexive muscle activation caused by sensory feedback and co-contraction can decrease the joint admittance, defined as the dynamic relation between input torque and output displacement [8]. Together with the passive viscoelasticity and mass these two mechanisms are the most important contributors to the joint dynamics. To better understand how posture and movement of a joint are controlled we want to obtain a description of the joint dynamics.

System identification techniques can be used to derive a description of the dynamical behaviour of a system from the input and output signals. Known perturbations can be supplied as input to the joint with the use of haptic robots. The output of the joint can be determined by measuring joint torque, joint angle and activation (EMG) of muscles. Since the human motor control system functions through a number of nested feedback loops [8] closed loop system identification techniques [9], [10] are needed to untangle cause and effect [11]. In posture control the range of motion of the joint is usually small. For this reason the system is assumed to behave linearly [12], [13], which enables the use of linear system identification techniques. The dynamics of the joint system can then be expressed with a Frequency Response Function (FRF) between the applied disturbance (e.g. torque perturbations from a haptic robot) and measured response (e.g. the joint angle). However, from the estimated dynamics it is not directly clear which component of the system contributes to the dynamics in what amount.

A. Modelling of joint dynamics

To better understand the role of an individual component (e.g. the muscle spindles) in the joint dynamics, neuromechanical models based on the known anatomy and physiology of the system are used. Neuromuscular models have to deal with the redundancy of the neuromuscular system. For example, for the 1DOF plantar-dorsiflexion motion in the ankle joint the tibialis anterior (TA), soleus (SOL) and gastrocnemius medialis and lateralis (GM and GL) can all contribute to the joint torque. Thus, a certain level of torque can be achieved with different activation combinations. All four muscles contributing to the joint torque have a length, stiffness and viscosity while usually only joint angle, torque and EMG are measured. As a result there is a small number of signals on which to fit a large number of parameters. One way to address this is to reduce the number of parameters with the implementation of a lumping method [14]. This is done for linear control models of the ankle, wrist and shoulder joint [1], [15], [16] where for example the passive viscoelasticity of all muscles is lumped together into one stiffness and one damping parameter and the muscle spindles can be represented as a lumped position and velocity feedback gain [1], [17]. A second way to address the indeterminacy is to provide additional equations. This is done in non-linear time domain models of the ankle joint, where additional equations based on anthropomorphic data are used to estimate the muscle length parameters from the measured ankle angle [18].

1) Joint angle and muscle contractile length: Muscle length is modelled in different ways: some assume muscle length to be proportional to ankle angle, while others assume that muscle length is equal to ankle angle filtered by a tendon of constant elasticity [8], [1]. Still others assume an infinite tendon stiffness but model a non-linear relationship between muscle contractile length and ankle angle as a result of a changing moment arm [19], [18].

To optimize the number of parameters in a neuromuscular model, it is necessary to identify the relevant structures that contribute to joint dynamics. In this case it is unknown what dynamic elements are necessary to model muscle contractile length. Therefore, this study wants to verify if muscle contractile length can be assumed proportional to the ankle angle during system identification experiments and which dynamics between ankle angle and muscle length should be included in models used for system identification.

2) Sensitivity of the muscle spindle: A modelled estimation of muscle length also has consequences for the estimation of the contribution of the muscle spindle. Muscle spindles are sensitive to muscle length and length change [20]. Their sensitivity can be altered by activation of the intrafusal muscle fibres from gamma motorneurons. However, in linear models the sensitivity of muscle spindles and Golgi tendon organs is assumed constant and the afferent feedback loop is represented by a set of gains and a time delay. This is in accordance with the fusimotor set hypothesis, which states that the CNS predicts a required sensitivity for the proprioceptors for upcoming movements and then sets the sensitivity to steady levels [21], [22]. The muscle stretch and stretch velocity are thus assumed to be the inputs to the muscle spindles, but during experiments they are not directly measured. They are derived from the joint angle instead.

In experiments that use transient perturbations to investigate reflexes typically two peaks can be distinguished in the EMG recording: a short latency response often labelled M1 and a longer latency response often labelled M2 [23]. Furthermore, in experiments with transient perturbations, larger joint velocities correlate with the short latency component of the stretch reflex [5], [24], [25]. If joint angle is proportional to muscle contractile length then the correlation of joint angle with the magnitude of the stretch reflex would be the same. However, if they are not proportional than one would be expected to predict the reflex size better than the other. Since muscle length is a more direct measure of input to the muscle spindle it is expected that muscle stretch velocity correlates better with the magnitude of the stretch reflex (as measured with EMG) than ankle velocity.

To be able to verify the assumption of a proportional ankle angle and muscle contractile length a measure of muscle contractile length is needed. This measurement can be obtained by recording ultrasound images of the muscles.

B. Ultrasound: measuring changes in muscle length

With ultrasound imaging the movement of muscle tissue can be visualized and the resulting images can be processed with a tracking algorithm to determine changes in muscle length. Methods to estimate tissue velocity from ultrasound images include spatial cross-correlation algorithms and gradient based optical flow algorithms such as the Lukas-Kanade method. With spatial cross-correlation algorithms changes in length as small as 5 μm could be detected, thus exceeding the resolution of the ultrasound transducer on its own [26]. This level of precision was achieved for small movements $(0.03 - 0.7^{\circ})$ and the same algorithm is unlikely to be capable of achieving the same precision for larger fast movements. Due to the more complex muscle deformations that occur between frames, such as shear, dilation and rotation, larger changes occur between images. As a result regions that were visible at the start may move out of the imaging plane. Thus, the cross-correlation algorithm has more difficulty recognizing the small features it tracks in the next frame [26]. Therefore, a tracking algorithm that tracks a more global movement of a larger region such as the Lucas-Kanade based *UltraTrack* [27], [28] algorithm which tracks the complete muscle region is more suitable for tracking larger and faster movements.

For faster muscle movements images should be recorded at a higher frame rate. However, the achievable frame rate is limited by a fundamental physical barrier: the speed of sound. In soft tissue the speed of sound is approximately 1540 m/s. When imaging at a depth of 5cm (required to see both GM and SOL) this means that the waiting time for one ultrasound beam to be send and returned is 0.065ms. To visualize complete muscle fascicles wide images are necessary, which are made with a large number of scan lines. With conventional line-by-line imaging and an image consisting of 256 scan lines this means that the maximum achievable

frame rate is physically limited at 60Hz. Higher frame rates up to 204Hz have been achieved with ultrasound equipment that has multi-beam imaging capabilities and can thus create multiple scan lines in one transmit beam [29], [30]. With plane-wave transmissions, which insonify a very large field of view with unfocused waves in a single transmission, muscles can be imaged at frame rates >1000Hz [31], [32]. However, the plane-wave technique comes at a cost in spatial resolution. The precision with which muscle contractile length can be measured depends not only on the spatial resolution of the ultrasound equipment, but also on the tracking algorithm used. The precision and accuracy that a tracking algorithm can achieve with a series of images of a certain resolution in turn depends on the type of movement that is imaged. Therefore, the feasibility of precisely measuring muscle length depends on the combination of the ultrasound equipment used, the tracking algorithm used and the movement that is imaged.

C. Research questions

The first goal of this study is to determine the feasibility of obtaining reliable measures of change in muscle length with plane-wave ultrasound imaging during two types of system identification techniques. The first technique applies continuous perturbations of a small amplitude. This allows more accurate quantification of the limb dynamics because a richer frequency range is applied [3]. The second technique applies transient perturbations. This technique allows a straightforward assessment of the reflex response.

The second goal is to test the validity of the assumption that contractile element length is proportional to ankle angle and to investigate the effect of this assumption on the prediction of reflex size. We aimed to answer the following two research questions:

- 1. What is the relationship between contractile element length and ankle angle during system identification experiments?
- 2. Is muscle velocity a better predictor of reflex size than ankle velocity?

Two experiments are conducted to answer these questions. In Experiment 1 continuous perturbations are used and in Experiment 2 transient perturbations are applied. First, it is hypothesized that ankle angle and contractile element length are not proportional for small amplitude continuous perturbations (Experiment 1) and during transient perturbation that evoke reflexes (Experiment 2). Second, it is hypothesized that muscle stretch velocity correlates stronger with the magnitude of the short latency stretch reflex than ankle velocity does (Experiment 2).

II. Method

Eight healthy participants (3 male and 5 female) with an age range of 24-17 years and height range of 1.67 - 1.87m volunteered. Four participants performed Experiment 1, the other four Experiment 2. All participants gave informed consent prior to the experiment and the study was approved by HREC the ethics committee of TU Delft.

A. Experimental set-up

1) Achilles: Disturbances were applied to the ankle joint with the Achilles ankle robot, which is a commercially available single axis robotic manipulator (Moog, Nieuw-Vennep, The Netherlands). Torque and angle measurements were recorded at 1024Hz. In front of the participant a computer screen was placed which was used to give feedback about performance during the experiments.

2) Disturbance signals: For Experiment 1, a continuous disturbance signal was designed in the frequency domain with equal power at 40 logarithmically spaced frequencies between 0.2Hz and 40Hz and a random phase. From 10,000 realizations, one 5s segment was chosen that had no outliers while having a distribution closest to a normal distribution. Six repetitions of the segment formed a 30s disturbance signal that was unpredictable in the time domain. A 5s segment can be seen in Figure 1.

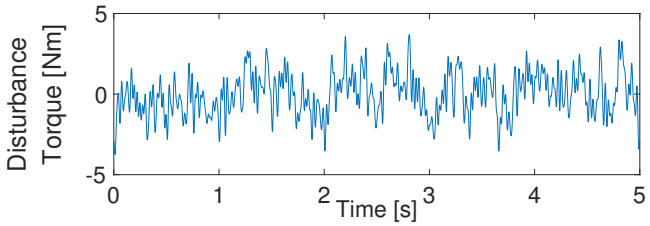

Fig. 1: The continuous torque disturbance applied during Experiment 1. The signal looks unpredictable and has no outliers.

For Experiment 2, a transient disturbance signal consisting of nine subsequent Ramp and Hold (RaH) disturbances was used. The first two RaHs had a velocity of 90 and $150^\circ/s$. These were used to let the participant adjust to the task again and were not recorded with ultrasound. Of the subsequent seven ramps one had a velocity of $8^\circ/s$ and two ramps each had velocities of 90, 150 and $200^\circ/s$. The order of these 7 ramps was randomized and there was a varying time interval (2.5±0.29s) between subsequent ramps. The return velocity was $20^\circ/s$. The signal can be seen in Figure 2.

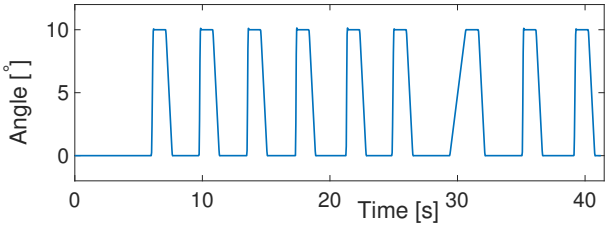

Fig. 2: The transient disturbance signal applied by the ankle robot during Experiment 2. It can be seen that the time interval between ramps varied which made the exact start of each disturbance unpredictable. The RaHs had ramp velocities of 8, 90, 150 and $200^\circ/s$

3) Electromyography: Differential surface electrodes and a TMSi amplifier (16 channel, Porti-7 8b8at) were used to record

EMG signals at a sample frequency of 1024Hz. The signals from the electrodes were amplified 20 times and filtered with a 1^{st} order low pass filter with -3db point at 4.8kHz before analog-to-digital (ADC) conversion. EMG electrodes were positioned according to SENIAM guidelines on the main dorsiflexor muscle, the tibialis anterior (TA) and the main plantarflexor muscles: the gastrocnemius medialis (GM), gastrocnemius lateralis (GL) and soleus (SOL). A ground electrode was placed on the knee cap. Before placing the electrodes the skin was locally cleaned with an abrasive skin preparation gel and shaved if necessary.

Fig. 3: Experimental set-up which shows the participants foot strapped to the ankle manipulator (*E*). The ultrasound probe and self-adhesive bandaging can be seen at *A*. The EMG electrodes attached to the skin are placed above the GM muscle as seen at *B* and above the SOL muscle as seen at *C* (Electrodes are also placed on the TA and GL, but not visible here). A ground electrode is placed on the kneecap at *D*.

4) Ultrasound: Ultrasound images were recorded with a Verasonics Vantage 256 research ultrasound and a Philips L12-5 50mm transducer which operated at a centre frequency of 7.8MHz. This research ultrasound uses plane-wave imaging which enables imaging with a greater time resolution than conventional ultrasound systems that image line-by-line. The RAM storage enabled recording 3000 frames consecutively. During Experiment 1 the frames were recorded at 130Hz for 23s and during Experiment 2 at 100Hz for 30 seconds. Recording depth was set to 50 mm to record both the GM and SOL muscle in one image. The location for the ultrasound probe was found by orienting the transducer perpendicular to the skin and parallel to the tibia to achieve a position in which the muscle fascicles of the GM lie in the image plane [33]. The ultrasound probe was held in place by a combination of Velcro straps together with an encasing of light clay and a self-adhesive bandage that was subsequently secured over the probe and around the leg as can be seen in Figure 3. Due to the RAM capacity of the ultrasound system the storage of a 3000 frame recording took 10 minutes as a result this was the minimum time between subsequent ultrasound recordings.

5) Data recording: To synchronize the data a TTL signal was sent from the analogue output of the ankle robot to the TMSi and to a NIDAQ 6211 USB device, which generated a square wave with a pulse frequency equal to the desired ultrasound frame rate. This square wave was send to the trigger input of the ultrasound system, where the falling edge of each block functioned as a trigger signal for the ultrasounds hardware sequencer to acquire a new frame. To determine the precise start and end of the ultrasound acquisition the square wave was also recorded on an analogue input channel of the ankle robot. A schematic overview of the recording set-up is shown in Figure 4.

B. Procedure

1) Participant preliminary measurements: Participants were seated in front of the ankle manipulator, with the foot in the anatomical position and the knee at a 45° from the anatomical position. The left foot was strapped onto the foot pedal of the manipulator with Velcro. Initial torque due to the weight of the leg and initial angle were recorded. Passive range of motion (ROM) was determined from the maximum angles reached while a slow monotonically increasing dorsiflexion torque and subsequently a plantarflexion torque with maximum values of 15Nm and 10Nm respectively were applied. Next, maximum voluntary contraction (MVC) was determined by instructing participants to push and pull as hard on the foot pedal as they could. Their current torque level was displayed on screen for motivation. The MVC was determined from the average of the maximum recorded torque value in plantar and dorsiflexion direction over two repetitions.

2) Experiment 1: Continuous: To ensure approximately linear dynamics during the position task the amplitude of the disturbances were scaled for every participant to achieve small ankle movements (1° SD). The same torque scaling factor was used for the relax task. The virtual stiffness of the ankle manipulator was increased to ensure that the movements were small enough (1° SD) during the relax task . Participants then performed 4 repetitions of the position task followed by 4 repetitions of the relax task, with 10 minute breaks between each repetition.

During position tasks a 3Nm bias torque was applied to ensure constant contraction of the plantarflexor muscles. To allow sufficient time to achieve the initial position, disturbances started after 13s.

3) Experiment 2: Transient: Participants performed the experiment in a relaxed and active condition. During the active condition they were required to deliver a 4Nm torque. There was no torque requirement for the relax task. Participants performed practice rounds of the active task until they consistently were able to reach and maintain the required torque level between disturbances. Participants performed 4 repetitions of the relax task with 10 minutes between the repetitions. Practice rounds for the active tasks were performed directly after the relax tasks was recorded while ultrasound data was being stored. Finally 4 repetitions of the active task were performed with 10 minute breaks in between recordings.

C. Task instruction

1) Experiment 1: Continuous: Participants were instructed to not intervene with disturbances during the relax task. For

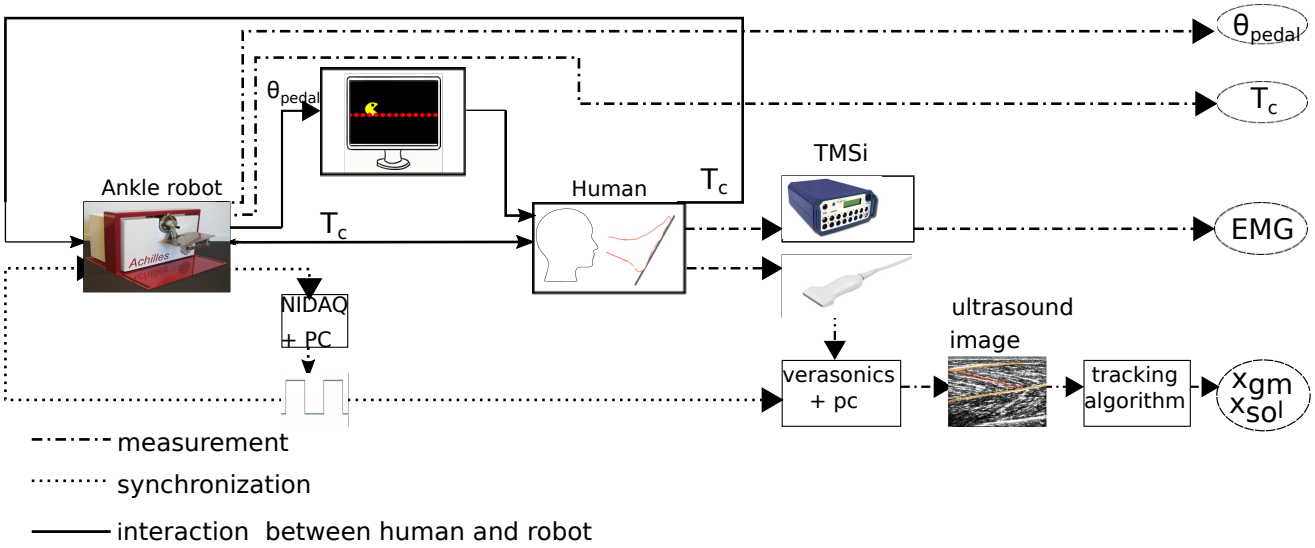

Fig. 4: Schematic of test set-up showing the interaction between human and the ankle robot through the contact torque T_c. Visual feedback of Experiment 1 is pictured were the foot pedal angle θ_{pedal} is used to give feedback to the participant. Measurements are made of T_c and θ_{pedal} with the ankle robot. The TMSi device is used to record the EMG measurements from the surface electrodes on the leg of the participant. The ultrasound probe images the SOL and GM muscles and the Verasonics ultrasound and a PC are used to make images out of the recording. These recordings are then processed with an image tracking algorithm to determine the contractile element length of the SOL x_{SOL} and GM x_{GM}. The synchronization process is initialized from the Achilles. A square wave is then generated and send to the ultrasound to trigger the recording of the ultrasound frames. The square wave is also recorded by the ankle robot. During Experiment 2 the scheme differs in the visual feedback which depend on the torque for Experiment 2 instead of the pedal angle.

the position task participants were instructed that the goal was to keep their foot in the same position. They were told that on screen feedback was given on how well they achieved this goal. It was said that if Pacman was "eating the red dots" then they were in the correct position. The visual feedback given is shown in Figure 5.

2) Experiment 2: Transient: First for the passive task participants were instructed to not intervene with the disturbances. Second for the active task they were instructed to contract their muscles such that they reached the torque level displayed on screen, but to not intervene with the disturbances. The visual feedback about the torque level is shown in Figure 6. Participants were told that when the foot returned to the initial position after a disturbances they should adjust the contraction of their muscles (if necessary) to again achieve the required torque level.

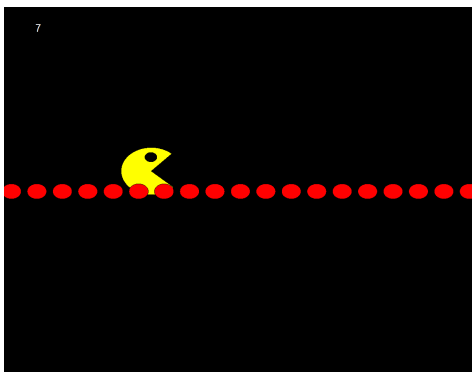

Fig. 5: Visual feedback given during the position task of Experiment 1. The measured foot pedal angle was low-pass filtered and displayed with a Pacman shaped figure. The required position was shown through red dots which moved from left to right over the screen, but had a constant vertical position.

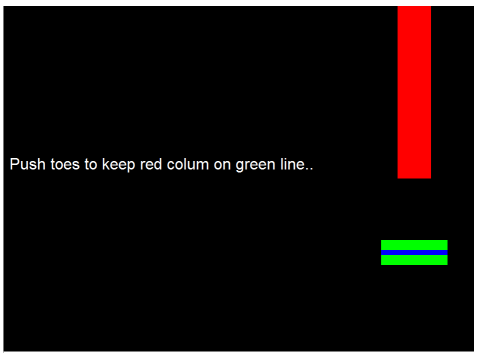

Fig. 6: Visual feedback given during the active task of Experiment 2. The red bar displays the measured ankle torque after it has been low-pass filtered. The green bar indicates the desired ankle torque $\pm 5\%$ and the blue line indicates the desired ankle torque $\pm 1\%$.

D. Data processing

1) Image processing: To determine the changes in muscle length from the ultrasound images an automatic tracking method developed by Cronin et al. [27] was used. The software called *Ultratrack* is based on a Lucas-Kanade optical flow algorithm with affine optic flow extension. Regions of interest (ROI) for the GM and SOL were marked on the first frame as is illustrated in Figure 7.

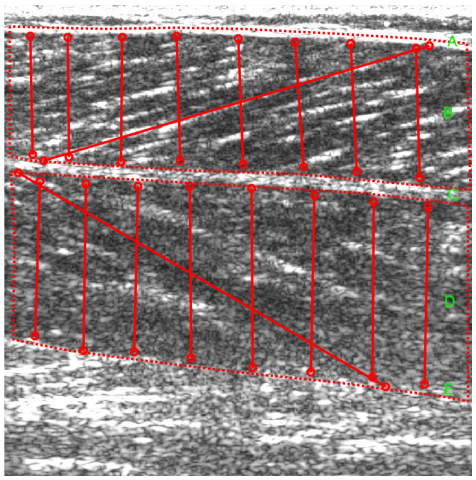

Fig. 7: The dotted red lines show the placement of the borders of the ROIs of the GM muscle (*B*) and the SOL muscle (*D*). The proximal aponeurosis of the SOL and GM (indicated with *A* and*E* respectively) are included in the ROI while the distal aponeuroses indicated at *C* are not. The small circles indicate the points that are tracked.

The proximal aponeurosis of the GM and SOL were included in their respective regions of interest, while their distal aponeurosis were not. The border between aponeurosis and muscle was instead chosen as the border of the respective muscle regions. In both ROIs a muscle fascicle was marked and eight approximately vertical lines running from positions close to the proximal aponeurosis to points close to the distal aponeurosis were placed along both region. The points of the eight vertical lines were used to determine the relative change in muscle length along the aponeurosis. The relative movement of the upper point of a straight line with respect to the lower component of the straight line was determined. The component of this movement in the direction of the aponeurosis was then found. To determine the muscle contractile length the average of the eight straight lines was taken.

2) Experiment 1: Continuous: The recorded trial was separated into the designed 5 second segments. The first and last segment were eliminated for each trial to remove transient effects, which left 16 segments per participant.

The ankle angle, ankle torque, external disturbance signal and change in contractile length of the GM and SOL were transformed to the frequency domain with the fast Fourier transform to estimate the spectral density for each segment. The spectral densities were subsequently averaged per participant. The dynamic relation between the contact force acting on the ankle and the resulting pedal angle was estimated

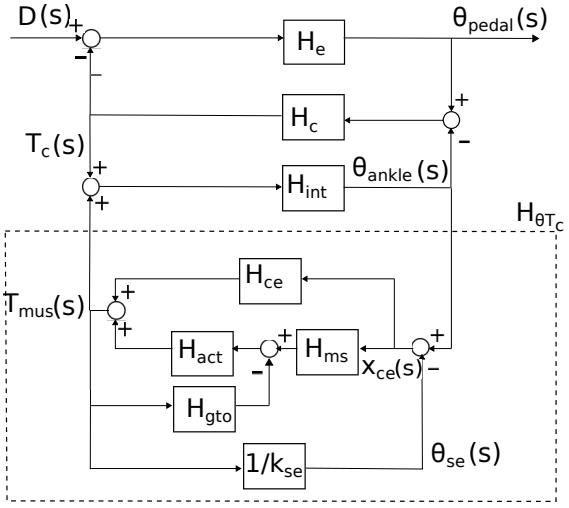

Fig. 8: Neuromuscular model that shows the contributions to the joint admittance in the frequency domain [8], [1]. The disturbance torque D is the input and the output is the foot pedal angle θ_{pedal}. The rotation of the joint is the result of the contact torque T_c and $Tmus$ muscle torque working on the limb. The mechanical admittance $\hat{H}_{\theta T}(f)$ describes the dynamic relation between the contact torque acting on the limb and the resulting rotation of the limb. The mechanical admittance consists of the viscoelasticity of all muscles H_{ce} and the afferent feedback. The GTO feedback H_{GTO} has the muscle torque T_{mus} as input and the muscle spindle H_{MS} the contractile element length x_{ce}. Activation dynamics transforms the activation into a contribution to T_{mus} . The contractile element length x_{ce} is in series with the tendon which is represented by a tendon elasticity k_se. As a result of the contact dynamics H_c the mechanical admittance differs slightly from the true admittance when estimated with the foot pedal angle instead of the ankle angle. The virtual dynamics of the Achilles robot form the environment H_e.

according to Equation 1.

$$\hat{H}_{\theta T}(f) = \frac{\hat{S}_{\theta D}(f)}{\hat{S}_{TD}(f)} \tag{1}$$

Here $\hat{S}_{\theta D}$ is the cross-spectral density of the external torque disturbance $D(f)$ and the angle of the manipulator $\theta_{pedal}(f)$ and $\hat{S}_{TD}(f)$ is the cross-spectral density between external torque disturbance $D(f)$ and the torque on the pedal T_c.

In the neuromuscular model in Figure 8 all muscles are lumped to form one viscoelastic element. Consequently there is one contractile element length. Two important plantar flexor muscles are imaged: the gastrocnemius and soleus. This gives two measures that contribute to the lumped contractile element length as seen in Figure 8. The obtained measures of x_{GM} and x_{SOL} are used to determine the dynamic relations between contact force and contractile element length of the gastrocnemius and soleus according to Equation 2.

$$\hat{H}_{x_{GM}T}(f) = \frac{\hat{S}_{x_{GM}D}(f)}{\hat{S}_{TD}(f)} \tag{2}$$

Where $\hat{S}_{x_{GM}D}$ is the cross-spectral density of the external torque disturbance $D(f)$ and the contractile element length of the GM muscle x_{GM}. To calculate the admittance for the soleus $\hat{H}_{x_{SOL}T}(f)$ the cross spectral density was calculated with the contractile element length of this muscle $\hat{S}_{x_{SOL}D}$ instead.

To quantify how much of the changes in ankle angle are reflected in the contractile length of the GM muscle x_{GM} the dynamic relation $\hat{H}_{x_{GM}\theta}$ between x_GM and θ_{pedal} was calculated according to Equation 3. The same calculation can be made for the soleus muscle.

$$\hat{H}_{x_{GM}\theta}(f) = \frac{\hat{S}_{x_{GM}D}(f)}{\hat{S}_{\theta D}(f)} \tag{3}$$

The calculation of admittance assumes linearity. Coherence was used to check this assumption. The coherence of the pedal position was calculated according to Equation 4. The coherence of contractile element length x_{GM} and x_{SOL} was calculated with Equation 5 here illustrated for the GM.

$$\hat{\gamma}^2_{\theta D}(f) = \frac{\left|\hat{S}_{\theta D}(f)\right|^2}{\hat{S}_{\theta\theta}(f)\hat{S}_{DD}(f)} \tag{4}$$

$$\hat{\gamma}^2_{x_{GM}D}(f) = \frac{\left|\hat{S}_{x_{GM}D}(f)\right|^2}{\hat{S}_{x_{GM}x_{GM}}(f)\hat{S}_{DD}(f)} \tag{5}$$

Welch averaging was used to determine the coherence values. A coherence value of 1 indicates a linear system without noise and lower values indicate a greater presence of noise and/or non-linearities. FRFs and coherences were only evaluated at the frequencies where the torque disturbance had power.

3) Experiment 2: Transient: For each trial possible 50Hz power line interference was removed, then the signal was high-pass filtered (1Hz cut-off, third-order Butterworth), rectified and smoothed with a low-pass filter (80Hz cut-off, third-order Butterworth). The data of each trial was then cut into segments containing the data of one ramp. The ultrasound images were analysed with the tracking algorithm per individual ramp.

RaH segments were removed from the analysis if the torque was not constant before ramp onset. Which was defined as a deviation larger than 10% from the required torque value in the 100ms before ramp onset. Segments were also removed if no obvious stretch reflex was present. To implement this the baseline EMG was determined as the EMG recording 500-100ms before the ramp onset. If the EMG peak after the ramp was not larger than the mean plus 3 times the standard deviation of the baseline EMG then the segment was removed. The segment was also removed if there was a large EMG peak (within 2 standard deviations of the reflex peak) present in the 100ms before the ramp onset.

The M1 and M2 response were then quantified by the area under the EMG signal at a time window of 1.040-1.065s and 1.070-1.010ms respectively and normalized with respect to the baseline EMG.

E. Statistical analysis

For Experiment 1 no statistical analysis was performed. For Experiment 2 the Pearson correlation coefficient is used to examine relationships between muscle velocity , disturbance velocity and reflex size. A significance level of $p<0.05$ was used. Average values are expressed as mean $\pm$ standard deviation.

III. RESULTS

A. Experiment 1: Continuous

1) Feasibility: We want to see if the measurements of muscle contractile length capture the actual movement of the muscles. Therefore, we look at how these measurements correlate with measured joint angle. Figure 9A shows a 5s segment recording of one participant during a relax task. In this recording x_{GM} and x_{SOL} oscillate in a very similar pattern as the recorded ankle angle. Furthermore, the recorded trajectory of x_{GM} and x_{SOL} looks only slightly less smooth than the recorded ankle angle. Figure 9B shows a segment of recording also made during a relax task, but from a different participant. Here x_{GM} again closely resembles the ankle angle trajectory, x_{SOL} however shows a drift that is not present in the ankle angle measurement.

Figure 10A shows a 5s recording made during a position task. Here the x_{SOL} measurement shows small high frequent oscillations that are not present in the θ_{pedal} measurement. However the pattern of larger lower frequent oscillations is similar for x_{GM}, x_{SOL} and θ_{pedal}. This is not the case for all recordings made during the position task. One case is seen in Figure 10C were a drift is present in the x_{GM} measurement which is not seen in θ_{pedal}. A second case can be seen in Figure 10 B were large 'jumps' are seen in the recording of x_{SOL} and especially x_{GM} that are not present in the recording of θ_{pedal}.

2) Proportionality: Figure 11 shows the ankle angle and contractile length of the soleus and gastrocnemius muscle averaged over all 16 data segments for one subject.

The pedal angle and contractile length of the soleus and gastrocnemius display a strong similarity in trajectory, especially for the relax task. During the position task the peaks in the ankle angle and muscle length trajectory sometimes almost overlap, while there is a larger difference in peak height at other points. Thus, scaling the ankle angle could never make it overlap completely with the muscle angle. This shows that ankle angle is not proportional to the muscle length during a position task.

Frequency domain identification

If θ_{pedal} is proportional to x_{SOL} and x_{GM} then $\hat{H}_{x_{GM}\theta}(f)$ and $\hat{H}_{x_{SOL}\theta}(f)$ would be constant values and could be represented with a straight line across al frequencies. Figure 12 shows $\hat{H}_{x_{GM}\theta}(f)$ and $\hat{H}_{x_{SOL}\theta}(f)$ for all four participants. Since drift was observed in some of the x_{SOL} and x_{GM} recordings the time domain segments were detrended before reconstructing the FRFs. In the case of the position task segments which showed 'jumps' like those in Figure 10B were also removed before reconstructing the FRFs. The frequency

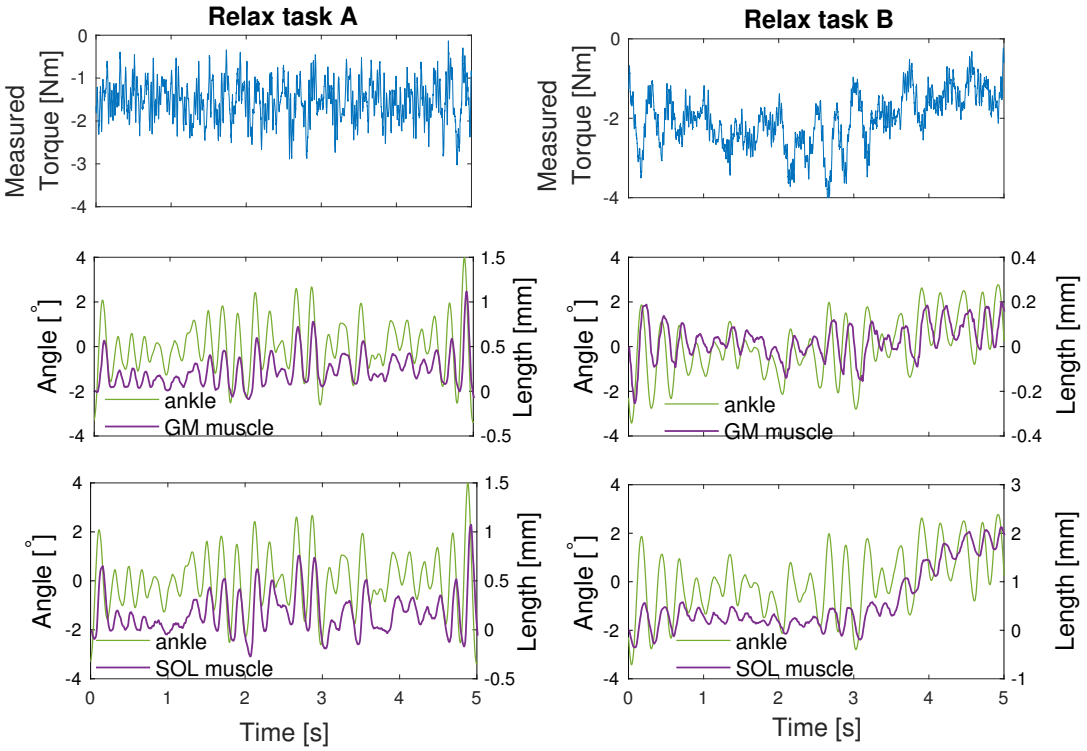

Fig. 9: Recordings of measured torque, ankle angle and changes in muscle lengths during a relax task. *A)* The overall trajectories of the ankle and the muscle lengths show strong similarities. *B)* The trajectory of the SOL muscle shows a drift that is not present in the GM muscle or the ankle angle recording.

response functions and coherences that were found when all recorded segments were used without deterending can be found in Appendix E.

It can be seen in Figure 12 that $\hat{H}_{x_{GM}\theta}(f)$ and $\hat{H}_{x_{SOL}\theta}(f)$ are not completely constant across all frequencies. A negative slope is seen across the lower frequencies for both tasks. To further determine the importance of this amount of deviation from a completely proportional relationship the effect on the estimate of the admittance should be examined.

If a proportional relationship exists between $\hat{H}_{x_{GM}T}$ and $\hat{H}_{\theta T}$ then $\hat{H}_{x_{GM}T}$ would be shifted a constant amount with respect to $\hat{H}_{\theta T}$ across all frequencies. Similarly if $\hat{H}_{x_{SOL}T}$ is proportional to $\hat{H}_{\theta T}$ then $\hat{H}_{x_{SOL}T}$ would be shifted a constant amount with respect to $\hat{H}_{\theta T}$. In Figure 13 the frequency response functions $\hat{H}_{\theta T}$,$\hat{H}_{x_{GM}T}$, $\hat{H}_{x_{SOL}T}$ and coherence $\hat{\gamma}^2_{\theta D}$, $\hat{\gamma}^2_{x_{GM}D}$ and $\hat{\gamma}^2_{x_{SOL}D}$ can be seen for one subject. It can be seen that the shape of the admittances are very similar.

Furthermore, we can observe in Figure 13 that $\hat{H}_{\theta T}$ is lower during the position task than the relax task as can be observed for all participants in Appendix B. $\hat{\gamma}^2_{\theta D}$ is very high across all frequencies for the relax task. During the position task $\hat{\gamma}^2_{\theta D}$ is lower for the lower frequencies and drops of more across the high frequencies. The high coherence for the relax task and lower coherence for the low frequencies during the position task can be seen across all subjects. From the figures of all participants (Appendix B) it can be determined that during the relax task the coherence $\hat{\gamma}^2_{\theta D} \geq 0.9$ for all participants and frequencies $\leq$29.6Hz. For the position task each participant has a $\hat{\gamma}^2_{\theta D} \geq 0.9$ for frequencies between 2.6-16.2Hz, and $\hat{\gamma}^2_{\theta D} \geq 0.8$ for frequencies between 1.4-2.6Hz. From Figure 12 it can be seen that the coherence of the muscle length is much lower than the coherence of the ankle angle during the position task. However, during the relax task the GM length shows a very high coherence for participant 1, 3, 4 and the SOL length also shows a high coherence for participant 1, 3, 4 but over a smaller frequency band.

From Figure 13 it is still difficult to judge the magnitude of the differences and similarities in the shape of the admittance graph due to the different heights of the graphs. Therefore, proportional difference are eliminated in Figure 14 . $\hat{H}_{x_{GM}T}$ and $\hat{H}_{x_{SOL}T}$ are multiplied with the average value of $|\hat{H}_{x_{GM}T}|/|\hat{H}_{x_\theta D}|$ and $|\hat{H}_{x_{SOL}T}|/|\hat{H}_{x_\theta D}|$ respectively and shown in one graph. It can be seen from Figure 14 that during the relax task the differences in the admittances are small for participant 1, 3 and 4 when only frequencies above 1Hz are considered. For the position task, the difference in admittance are small for participant 2 and 4 for frequencies above 1Hz. For the other two participants larger differences are seen.

During the position task the standard deviation of the ankle angle around the mean for all subjects and trials was on average 0.90$\pm$0.25° and the range of the applied scaling factor was 0.65-1.3. During the relax task the ankle movement

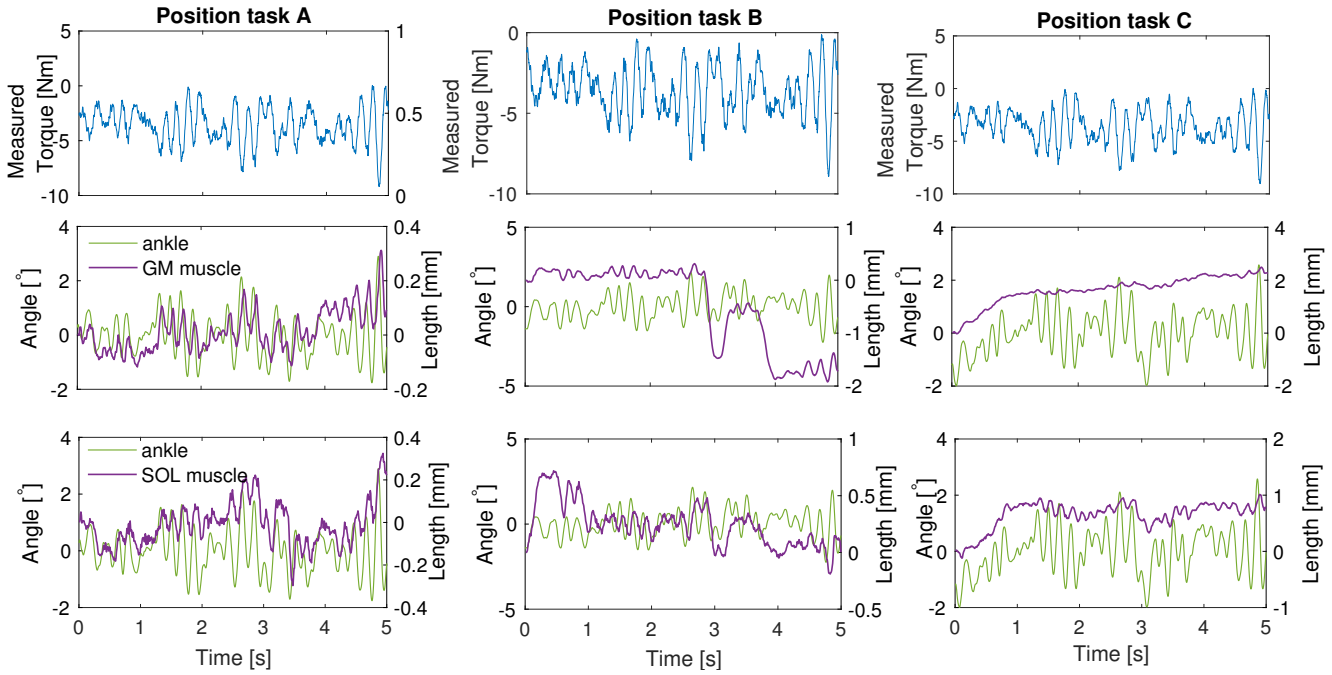

Fig. 10: Some recordings of the muscle length show larger similarity to the measured ankle angle than other recordings. *A)* Strong similarity between ankle angle and muscle length recordings. *B)* The muscle length trajectory of the SOL and especially the GM show 'jumps' that are not seen in the recorded ankle angle. *C)* The recorded muscle lengths show a drift that is not seen in the recorded ankle angle.

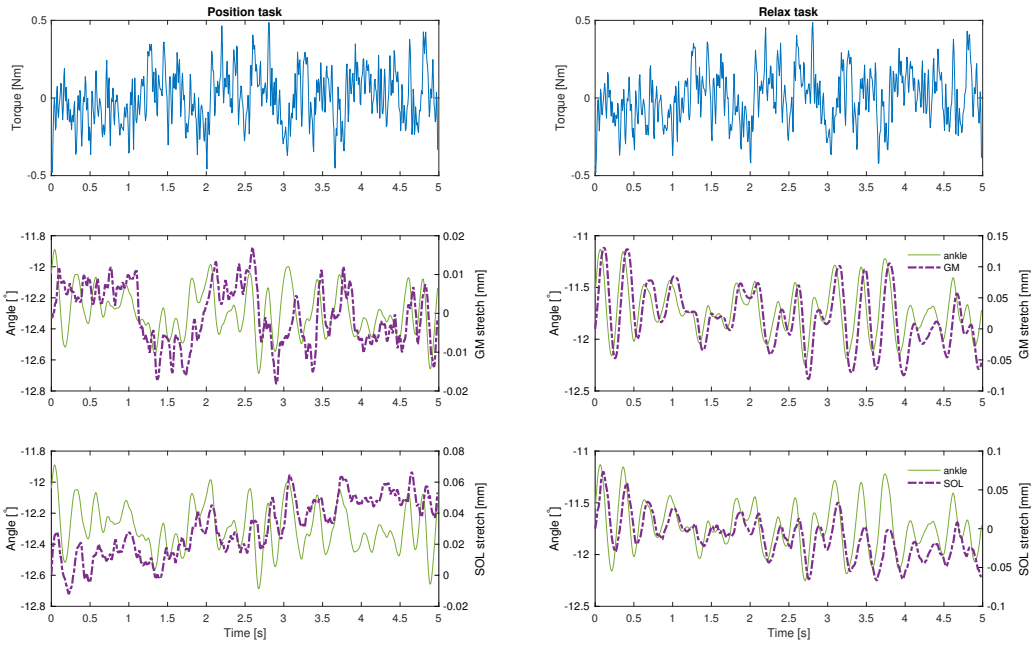

Fig. 11: Ankle angle and muscle length are not completely proportional especially during the during the relax task. Measurements are averaged over all 16 data segments for one subject. *Top panels)* Measured torque. *Middle panels)* The ankle angle and contractile length of the gastrocnemius muscle and *Bottom panels)* soleus.

had on average a standard deviation of 1.06 $\pm$0.16°, for which a virtual stiffness ranging from 35-100Nm/rad was applied. The subjects had an average MVC of 32.4$\pm$ 9.5Nm in plantarflexion and 27.3$\pm$6.1Nm in dorsiflexion.

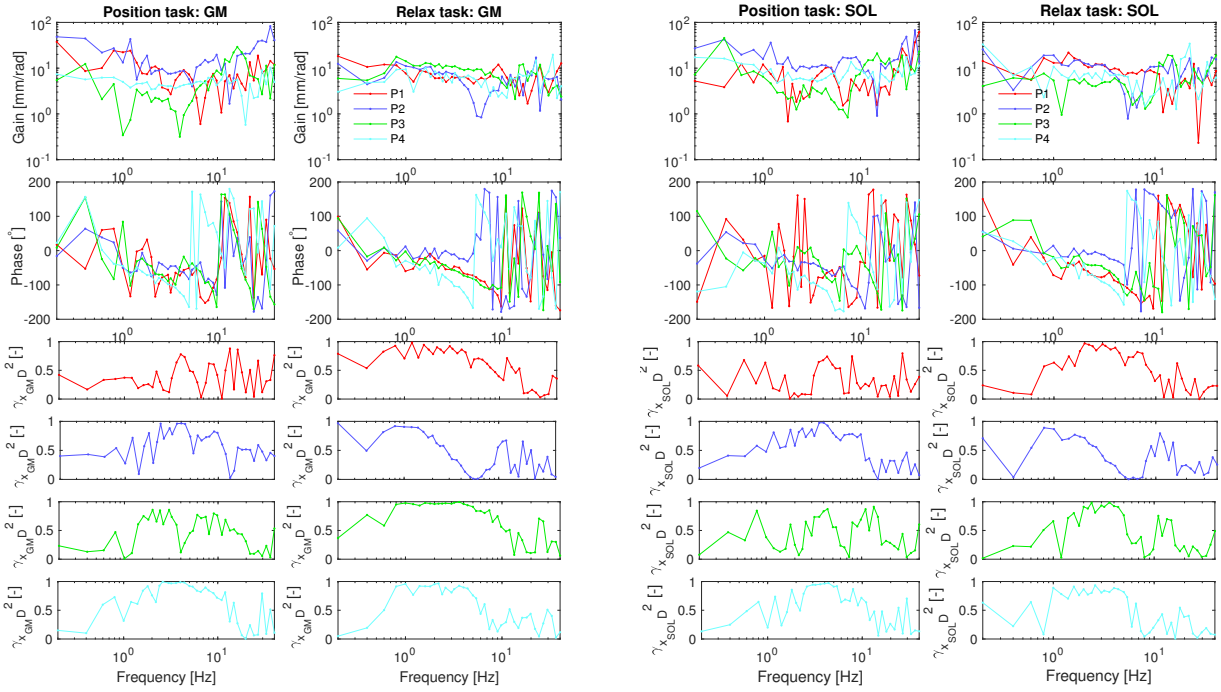

Fig. 12: $\hat{H}_{x_{GM}\theta}(f)$ and $\hat{H}_{x_{SOL}\theta}(f)$ during the position and relax task are displayed for all 4 participants, were the data of each participant is represented with a different colour. The first row shows the gain of $\hat{H}_{x_{GM}\theta}(f)$ and $\hat{H}_{x_{SOL}\theta}(f)$ for the position and the relax task. For the position task a negative slope can be seen across the lower frequencies. The lines of the relax task closer approximate a straight line. The second row shows the phase of $\hat{H}_{x_{GM}\theta}(f)$ and $\hat{H}_{x_{SOL}\theta}(f)$. Row 3-6 show the coherence of x_{SOL} and x_{GM} were each row represents a separate participant. The coherences are generally higher during the relax task.

B. Experiment 2: Transient

1) Feasibility: During the RaH perturbations the trajectories of ankle angle and contractile element length are very dissimilar as can be seen in Figure 15. The variability of the measured response of the muscle contractile length within subjects is low as can be seen from the similar shape of all repetitions of the same ramp velocity for individual participants (Appendix D). The figures in Appendix C also illustrate that the measured responses between participants differ in the amount of oscillation that is present in the muscle length trajectories.

2) Proportionality: From Figure 15 it is clearly visible that muscle length is not proportional to ankle angle as oscillations are present in the measured GM and SOL length (panel B and C) that are not seen for the ankle angle (panel A). This is true both for the active and relax task.

3) Reflexes: In Figure 15 the averaged ramp responses can be seen for one subject. For this subject a larger velocity of the ramp disturbance corresponds with a larger fascicle velocity (panel E and F) directly after onset (0.014s after the disturbance) and a larger EMG peak (panel G and H). The relationship between M1, M2 and stretch velocity measured directly after perturbation onset for all four participants during the active task is visualized in Figure 16. The relationship of M1 and M2 with joint velocity can be seen in Figure 17. The points of the different participants lie closer together in the M1-GM stretch plot than in the M1-perturbation velocity plot.

In Table I the correlation coefficients are summarized for the active condition. It can be seen that for the GM a strong and significant correlation can be found between stretch velocity and M1 as well as between stretch velocity and M2. M2 also correlates strongly with perturbation velocity, but for M1 a significant correlation with perturbation velocity is not found. For the soleus the only significant correlation found is a strong correlation between perturbation velocity and M2.

TABLE I: Correlations between perturbation velocity, muscle stretch velocity and reflex size for the active task.

	GM	SOL
Stretch - M1	0.664 (0.018)	0.441 (0.151)
Stretch - M2	0.893 (0.000)	0.540 (0.070)
Perturbation Vel.- M1	0.402 (0.195)	0.430 (0.163)
Perturbation Vel.- M2	0.760 (0.004)	0.903 (0.000)
Stretch - Perturbation Vel.	0.524 (0.080)	0.596 (0.041)

Values are given as follows: Correlation coefficient (p-value).

For the relax task the correlations are summarized in Table

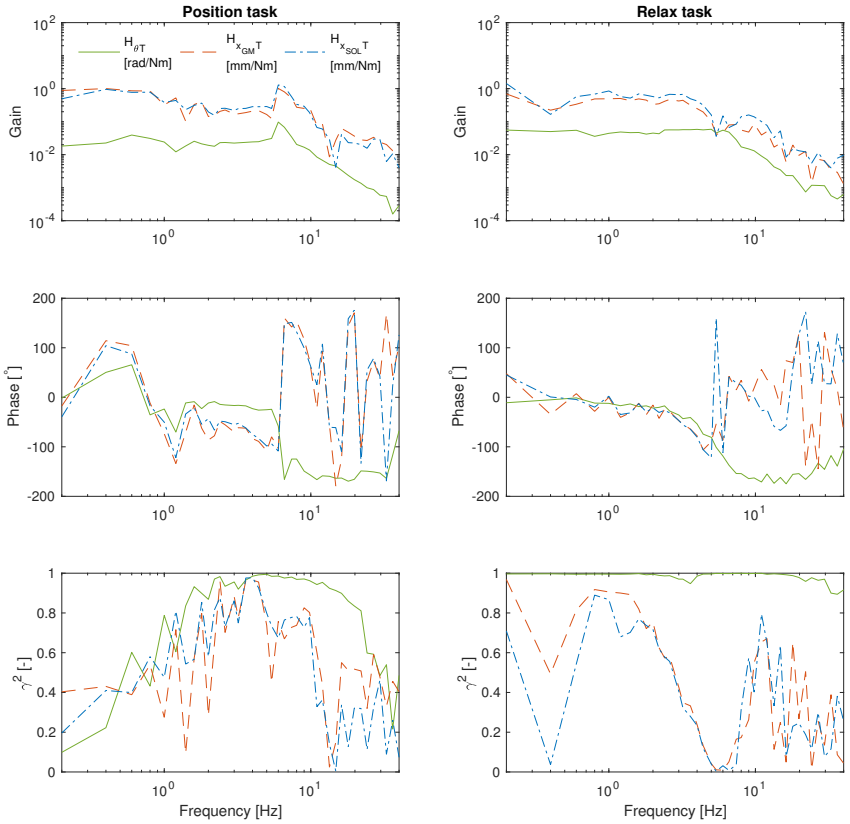

Fig. 13: The gains of $\hat{H}_{x_{GM}T}$and $\hat{H}_{x_{SOL}T}$ have a similar shape to the gain of $\hat{\gamma}^2_{\theta D}$ as can be seen for both the position and relax task. The coherence of the ankle angle is high during the relax task and lower during the position task. The coherence of the muscle length is lower than the coherence of the ankle angle for both muscles and both tasks.

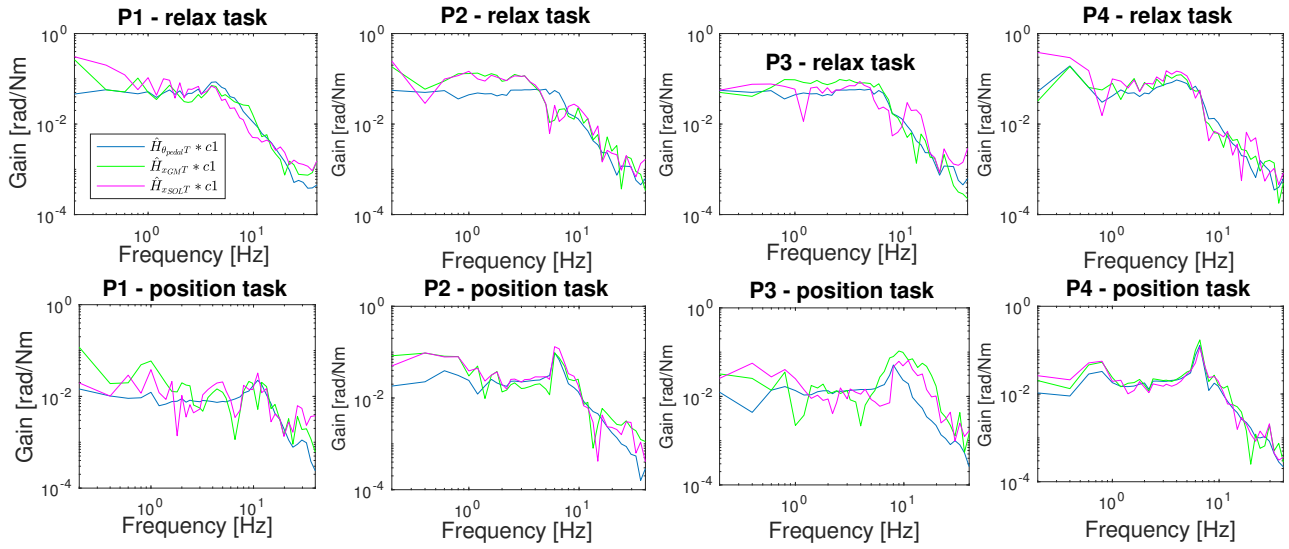

Fig. 14: $\hat{H}_{x_{GM}T}$ and $\hat{H}_{x_{SOL}T}$ are multiplied with the average value of $|\hat{H}_{x_{GM}T}|/|\hat{H}_{x_\theta D}| = c1$ and $|\hat{H}_{x_{SOL}T}|/|\hat{H}_{x_\theta D}| = c2$ respectively to eliminate differences in admittance that can be explained by proportional difference between ankle angle and muscle length.

II. For both muscles the correlation of M1 with muscle stretch is much weaker than in the pre-contracted condition. A significant but not very strong correlation is found between perturbation velocity and the M1 response of the soleus. Stronger correlations are found between the perturbation velocity and the M1 and M2 response of the gastrocnemius medialis.

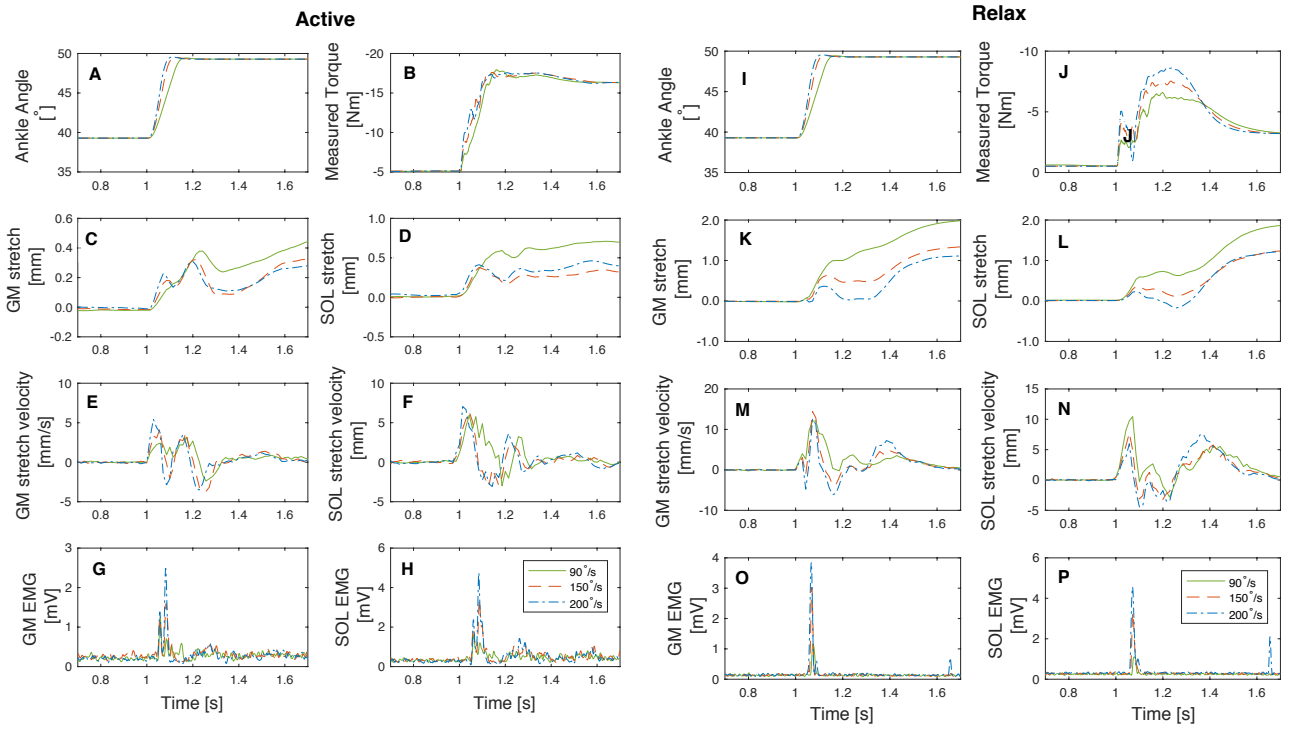

Fig. 15: The average response of one subject to RaH perturbations of different velocity during a relax and active task. It can be seen that larger perturbation velocity corresponds with a larger GM stretch velocity during the active task (Panel C). It can also be seen that larger perturbation velocities correspond with higher peaks in the EMG trajectories of both the GM and the SOL during the active and relax task.

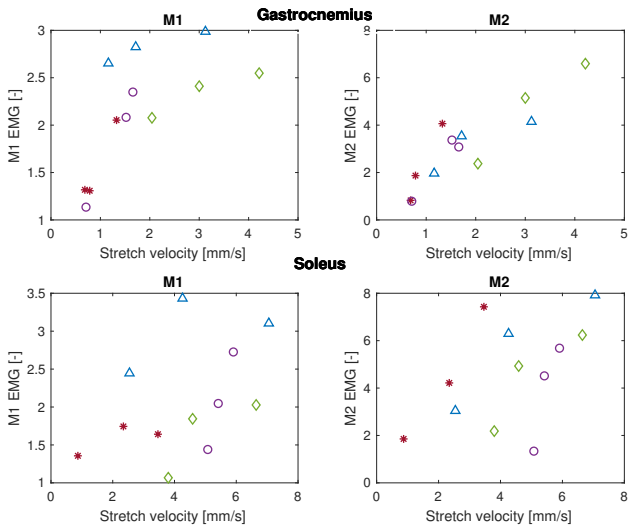

Fig. 16: Average stretch velocities of the GM and SOL are plotted against the M1 and M2 response during the active task. Every different symbol is a different participant. The relationship of SOL with M1 and M2 is more spread apart than the relationship of GM with M1 and M2.

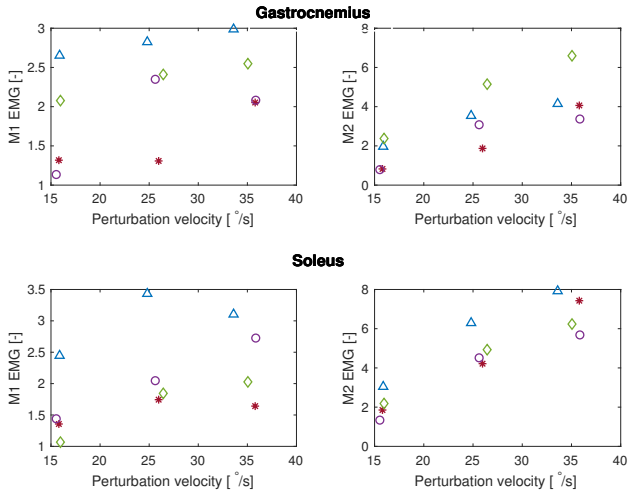

Fig. 17: Average ankle joint velocity of the GM and SOL are plotted against the M1 and M2 response during the active task. Every different symbol is a different participant. In the graph bottom right graph it can be seen that the data points representing the relationship between the M2 response of the soleus and the perturbation velocity lie approximately along a straight line.

The participants of Experiment 2 had an average MVC of 22.3± 6.7Nm in plantarflexion and 24.8±1.6Nm in dorsiflexion.

TABLE II: Correlations between perturbation velocity, muscle stretch velocity and reflex size for the relax task.

	GM	SOL
Stretch - M1	0.323 (0.306)	0.492 (0.104)
Stretch - M2	0.746 (0.005)	0.444 (0.148)
Perturbation Vel.- M1	0.556 (0.061)	0.585 (0.046)
Perturbation Vel.- M2	0.697 (0.012)	0.277 (0.383)
Stretch - Perturbation Vel.	0.389 (0.211)	0.374 (0.231)

Values are given as follows: Correlation coefficient (p-value).

IV. Discussion

The first goal of this study was to determine the feasibility of using plane-wave ultrasound to make recordings of muscle length during two system identification techniques: continuous and transient disturbances. It was shown that muscle contractile length measurement is possible for both types of perturbations. The second goal was to use the muscle length measurements to investigate the assumption of a proportional relationship between muscle length and ankle angle. It was hypothesized that ankle angle and muscle contractile length are not proportional for both disturbance types. It was shown that the assumption of proportionality between muscle length and ankle angle does not hold during the transient perturbations, but is a good approximation when participants relax during small amplitude continuous perturbations. Furthermore, it was hypothesized that muscle stretch velocity correlates stronger with the size of the short latency reflex than with ankle velocity. A stronger correlation of M1 with stretch velocity than with perturbation velocity was shown for the gastrocnemius medialis.

1) Feasibility of combining ultrasound and system identification: During a system identification experiment with small amplitude continuous perturbations the muscle length measurement showed a high coherence during the relax task. This indicates that the influence of random measurement noise is low. The lower coherence of x_{GM} and x_{SOL} during a position task indicates that a larger amount of non-linear behaviour between the measured muscle length and the applied disturbance is present than during the relax task. This can be caused by non-linear behaviour of the system or be a result of the quality of the measurement signals. The high coherence between disturbance and pedal angle indicates that these measurements have a low level of noise. However, the low level of noise in x_{GM} and x_{SOL} measurement during the relax task does not indicate that the same low level of noise is present in the muscle length measurement during the position task. The reason for that is that the performance of the tracking algorithm depends on the type of movement that is imaged. Larger more rapid movements made during the position task can be harder to track. There are two reasons for this. Firstly, larger movements between frames can cause poor performance of the tracking algorithm. Secondly, out of plane movement of the muscle can cause the brightness to change between images thereby failing a key assumption of the tracking algorithm [28].

A further source of inaccuracy in the muscle length measurements can result from the fact that the tracking algorithm calculates change relative to the preceding frame. This can cause errors to accumulate over time. In the recording shown in Figure 10C the motion looks like it could be caused by drift. However, drift is not present in all recordings of the same participant with the same task. Also, the drift in muscle length can be present in the GM while it is not present in the SOL. The drift in the muscle length measurement can be the result of error accumulation by the tracking algorithm or it could be the actual behaviour of the muscle. For example, the subject could be slowly increasing the level of co-contracting thereby reducing the length of the muscle. This could be investigated dy determining if the drift in muscle length correlates with the EMG of the muscle.

In this study it was attempted to reduce the influence of drift in the frequency domain analysis by detrending the recorded segments of Experiment 1. This improved $\hat{\gamma}^2_{x_{GM}D}$ for the relax task of all participants as can be seen when comparing Figure 12 with Appendix E. For participants 3 and 4, $\hat{\gamma}^2_{x_{SOLD}}$ during the relax task was also improved by detrending. However in the case of participant 1 detrending decreased $\hat{\gamma}^2_{x_{SOLD}}$. Deterending improved the coherence for participant 3 during the position task. However, removing the segments with 'jumps' such as seen in Figure 10B did not result in a clear improvement of $\hat{\gamma}^2_{x_{GMD}}$ or $\hat{\gamma}^2_{x_{SOLD}}$ as can be seen when comparing Figure 12 with Appendix E . This lack of decrease in the amount non-linear behaviour in the measured muscle length indicates that significant non-linear behaviour besides the 'jumps' is present in the measurements.

For future experiments it is recommended to analyse the images with a tracking algorithm that does not use the preceding frame as a reference, or an absolute reference, but a reference frame that is changed in steps.

The feasibility of using plane-wave ultrasound to acquire 2D images of skeletal muscle has been shown before by Deffieux et al. [34], [31]. Both parallel and perpendicular to the muscle fibres 2D images were acquired to show the electromechanical waves propagating in the biceps. A different analysis was performed on the images and the images were acquired of muscle movement in response to electrical stimulation instead of mechanical perturbation as was done in this study. High frame rate ultrasound recordings (204Hz) have been acquired of the gastrocnemius during transient disturbance with ultrasound equipment with multi-beam imaging capabilities by Cronin et al. [29].

2) Proportionality between ankle angle and muscle length: During the position task the coherence of the muscle length measurements is low and it is unclear what part of the non-linearity in the measurement is due to the image tracking method and what part is due to the underlying behaviour of the muscle. Therefore, the extend of the non-proportional behaviour between muscle length and ankle angle during the position task cannot be reliably determined from this study. A further investigation should not only use a tracking algorithm less prone to drift, but could also quantify the effect that the assumption of proportionality has on the estimation of model parameters. Furthermore, this study does not take into account that the measured pedal angle is not the same as the

ankle angle. With parametric system identification techniques the contact dynamics between the ankle angle and the foot pedal angle can be modelled as illustrated in Figure 8 and taken into account. It should however be considered that the gastrocnemius medialis and lateralis, the soleus and tibialis anterior together give the lumped behaviour of the contractile element length seen in the model in Figure 8, while only two of these muscles were imaged in this study.

3) Reflex prediction: It is generally agreed that the M1 response originates from the monosynaptic Ia afferent reflex pathway [5] where the Ia afferent provides information on the muscle stretch velocity. As a result a strong correlation between muscle stretch velocity and M1 size would be expected. This study found a strong correlation between muscle stretch velocity of the gastrocnemius medialis and the size of M1. However, Cronin et al. [29] saw a weak correlation between muscle stretch velocity and the size of M1. Which let them to propose them to propose that the SLR is triggered by a transmission of vibratory stimuli through the lower limb rather than the exceeding of a certain threshold of muscle fibre stretch. At least three reasons could explain the difference in findings between these studies. First of all this study used disturbances of different velocities while Cronin et al. [29] used disturbances that had the same velocity but differed in amplitude and also varied the pre-activation level. Secondly, the muscle velocity was evaluated at a different measurement interval after perturbation. This study used muscle velocity 0.014s after disturbance onset while Cronin et al. measured disturbance velocity 0.005s after perturbation onset. Thirdly, this study used change in length along the aponeurosis while Cronin et al. [29] used fascicle velocity.

The origin of M2 response is more complex and still debated. For a constant disturbance amplitude M2 has been shown to actually decrease with disturbance velocity for the flexor carpi radialis muscle [5] and shown to depend on perturbation duration. However, Thilmann et al. [25] found an increase in the size of the M2 response of the triceps surae with increased disturbance velocity at the same disturbance amplitude. Which is in accordance with the findings of this study which showed an increase of M2 size with increased perturbation velocity.

4) Experimental considerations: It is important to remark that the feasibility of recording ultrasound measurements during system identification experiments, highly depends on the specifications of the ultrasound system. For future research that uses this experimental set-up, a short overview of problem solving is given in Appendix A. This could help with future selection of a suitable ultrasound system. The most important factors to be considered when setting-up ultrasound recordings during system identification experiments are: (1) the frame rate of the ultrasound system, (2) the number of consecutive frames the apparatus can record, and the (3) synchronization of the ultrasound recording with the other measurements that are recorded.

The set-up of this study was designed to achieve a consistent interval between the recording of ultrasound frames by triggering the acquisition of each frame. The trigger signal was recorded with the Achilles robot to achieve synchronization with the other measured signals. However, synchronization between the ultrasound recording and the other measurements was not achieved at the desired level. From the recordings with transient perturbations it was estimated that at the last ramp of each trial the ultrasound measurement had developed a lag of 0.14s with respect to the other measurements. Due to the imperfect synchronization the data from Experiment 2 had to be realigned. For each ramp the first significant deviation in velocity after perturbation onset was found. For active conditions it had to be larger than the mean plus three times the standard deviation of the muscle length before ramp onset and for passive conditions larger than the mean plus five times the standard deviation. This point of first significant deviation was used as the first time step after perturbation onset. This method failed visibly for four ramps, which were aligned by hand. For Experiment 1 no realignment was performed.

The data processing required to transform ultrasound recordings to muscle length measurements makes it less convenient than measuring the joint angle and torque. Even though an image tracking algorithm is used image processing still takes time. For the processing of Experiment 2 for example, the regions of interest and accompanying tracking lines had to be marked on 224 images. For larger studies algorithms that automate the segmentation and selection of relevant features [35] could be useful.

In this study the highest frame rate used was 130Hz. However, with plane-wave imaging recordings up to at least a 1000Hz could be made which have the same image quality as the recordings that were made at 130Hz. In the current study RAM memory of the ultrasound system limited the recoding length to 3000 frames which prevented recording with a higher frame rate at the required duration. However with shorter recordings (or more RAM) it is possible to investigate the muscle response even shorter after the disturbance onset.

V. Conclusion

It was shown that it is possible to use plane-wave ultrasound recordings to make low noise measurements of muscle length during system identification experiments with continuous as well as transient perturbations. To improve the muscle length measurements a tracking algorithm less prone to drift should be used.

Ankle angle and muscle length can be assumed proportional, when small amplitude (1° SD) continuous perturbations are applied to the ankle joint and the subject is asked to relax. This study suggest the assumption also holds during a position task, however more research with better image tracking is needed to confirm this. Furthermore, this study shows that ankle angle and muscle length are not proportional during RaH perturbations of a high velocity ($> 90^\circ/s$).

Finally it shows that muscle length is a better predictor for the M1 response elicited in the GM muscle by a RaH perturbation than perturbation velocity if the muscle is pre-contracted.

Acknowledgment

I would like to thank Winfred Mugge, Alfred Schouten and Karen Rodriguez Hernandez for all their guidance, encourage-

ment and feedback. Verya Daeichin, I would like to thank for all his time and effort in facilitating the experimental set-up.

REFERENCES

[1] W. Mugge, D. A. Abbink, A. C. Schouten, J. P. A. Dewald, and F. C. T. Van Der Helm, "A rigorous model of reflex function indicates that position and force feedback are flexibly tuned to position and force tasks," *Experimental Brain Research*, vol. 200, no. 3-4, pp. 325–340, 2010.

[2] B. Chen, Y. J. Lee, and A. S. Aruin, "Control of grip force and vertical posture while holding an object and being perturbed," *Experimental Brain Research*, vol. 234, no. 11, pp. 3193–3201, 2016.

[3] E. De Vlugt, A. C. Schouten, and F. C. T. Van Der Helm, "Closed-loop multivariable system identification for the characterization of the dynamic arm compliance using continuous force disturbances: A model study," *Journal of Neuroscience Methods*, vol. 122, no. 2, pp. 123–140, 2003.

[4] M. M. Mirbagheri, H. Barbeau, and R. E. Kearney, "Intrinsic and reflex contributions to human ankle stiffness: Variation with activation level and position," *Experimental Brain Research*, vol. 135, no. 4, pp. 423–436, 2000.

[5] J. Schuurmans, E. De Vlugt, A. C. Schouten, C. G. M. Meskers, J. H. De Groot, and F. C. T. Van Der Helm, "The monosynaptic Ia afferent pathway can largely explain the stretch duration effect of the long latency M2 response," *Experimental Brain Research*, vol. 193, no. 4, pp. 491–500, 2009.

[6] M. L. Latash and V. M. Zatsiorsky, "6 - Reflexes ," in *Biomechanics and Motor Control*. San Diego: Academic Press, 2016, pp. 99–120. [Online]. Available: https://www.sciencedirect.com/science/article/pii/B9780128003848000065

[7] A. Bear, Mark F., Connors, Barry W. Paradiso, Michael, *Neuroscience Exploring the Brain*, 3rd ed. Lippincott Williams & Wilkins, 2007.

[8] A. C. Schouten, W. Mugge, and F. C. T. van der Helm, "NMClab, a model to assess the contributions of muscle visco-elasticity and afferent feedback to joint dynamics," *Journal of Biomechanics*, vol. 41, no. 8, pp. 1659–1667, 2008.

[9] D. T. Westwick and E. J. Perreault, "Closed-loop identification: Application to the estimation of limb impedance in a compliant environment," *IEEE Transactions on Biomedical Engineering*, vol. 58, no. 3 PART 1, pp. 521–530, 2011.

[10] H. Van Der Kooij, E. Van Asseldonk, and F. C. Van Der Helm, "Comparison of different methods to identify and quantify balance control," *Journal of Neuroscience Methods*, vol. 145, no. 1-2, pp. 175–203, 2005.

[11] C. G. M. Meskers, J. H. de Groot, E. de Vlugt, and A. C. Schouten, "NeuroControl of movement: system identification approach for clinical benefit." *Frontiers in integrative neuroscience*, vol. 9, no. September, p. 48, 2015. [Online]. Available: http://www.pubmedcentral.nih.gov/articlerender.fcgi?artid=4561669{\&}tool=pmcentrez{\&}rendertype=abstract

[12] R. E. Kearney and I. W. Hunter, "System identification of human stretch reflex dynamics: Tibialis anterior," *Experimental Brain Research*, vol. 56, no. 1, pp. 40–49, 1984.

[13] E. de Vlugt, A. C. Schouten, V. D, and F. C. T. er Helm, "Adaptation of reflexive feedback during arm posture to different environments," *Biological Cybernetics*, vol. 87, no. 1, pp. 10–26, 2002.

[14] J. Mizrahi, "Mechanical impedance and its relations to motor control, limb dynamics, and motion biomechanics," *Journal of Medical and Biological Engineering*, vol. 35, no. 1, pp. 1–20, 2015.

[15] F. C. T. Van Der Helm, A. C. Schouten, E. De Vlugt, and G. G. Brouwn, "Identification of intrinsic and reflexive components of human arm dynamics during postural control," *Journal of Neuroscience Methods*, vol. 119, no. 1, pp. 1–14, 2002.

[16] A. Klomp, J. H. De Groot, E. De Vlugt, C. G. M. Meskers, J. H. Arendzen, and F. C. T. Van Der Helm, "Perturbation amplitude affects linearly estimated neuromechanical wrist joint properties," *IEEE Transactions on Biomedical Engineering*, vol. 61, no. 4, pp. 1005–1014, 2014.

[17] A. C. Schouten, E. D. Vlugt, J. J. B. V. Hilten, and F. C. T. V. D. Helm, "Quantifying Proprioceptive Reflexes During Position Control of the Human Arm," *The Hand*, vol. 55, no. 1, pp. 311–321, 2008.

[18] K. L. de Gooijer-van de Groep, E. de Vlugt, J. H. de Groot, H. C. M. van der Heijden-Maessen, D. H. M. Wielheesen, R. M. S. van Wijlen-Hempel, J. H. Arendzen, and C. G. M. Meskers, "Differentiation between non-neural and neural contributors to ankle joint stiffness in cerebral palsy." *Journal of neuroengineering and rehabilitation*, vol. 10, no. 1, p. 81, 2013. [Online]. Available: http://www.pubmedcentral.nih.gov/articlerender.fcgi?artid=3737029{\&}tool=pmcentrez{\&}rendertype=abstract

[19] E. de Vlugt, J. H. de Groot, K. E. Schenkeveld, J. H. Arendzen, F. C. T. van der Helm, and C. G. M. Meskers, "The relation between neuromechanical parameters and Ashworth score in stroke patients." *Journal of neuroengineering and rehabilitation*, vol. 7, p. 35, 2010.

[20] M. L. Latash and V. M. Zatsiorsky, "Posture," in *Biomechanics and Motor Control*. Academic Press, San Diego, 2016, ch. 14 - Postu, pp. 327–238. [Online]. Available: http://linkinghub.elsevier.com/retrieve/pii/B9780128003848000144

[21] a. Prochazka, M. Hulliger, P. Zangger, A. K., and K. Appenteng, "'Fusimotor set': new evidence for alpha-independent control of gamma-motoneurones during movement in the awake cat." *Brain research*, vol. 339, pp. 136–140, 1985.

[22] A. Prochazka, "Sensorimotor Gain-Control - A Basic Strategy of Motor Systems," *Progress in neurobiology*, vol. 33, no. 4, pp. 281–307, 1989.

[23] W. G. Tatton and R. G. Lee, "Evidence for abnormal long-loop reflexes in rigid Parkinsonian patients," *Brain Research*, vol. 100, no. 3, pp. 671–676, 1975.

[24] W. Mugge, A. G. Munts, A. C. Schouten, and F. C. T. van der Helm, "Modeling movement disorders-CRPS-related dystonia explained by abnormal proprioceptive reflexes," *Journal of Biomechanics*, vol. 45, no. 1, pp. 90–98, 2012. [Online]. Available: http://dx.doi.org/10.1016/j.jbiomech.2011.09.024

[25] A. F. Thilmann, M. Schwarz, R. Topper, S. J. Fellows, and J. Noth, "Different mechanisms underlie the long-latency stretch reflex response of active human muscle at different joints." *The Journal of Physiology*, vol. 444, pp. 631–643, 1991. [Online]. Available: http://www.ncbi.nlm.nih.gov/pmc/articles/PMC1179953/{\%}5Cnhttp://www.ncbi.nlm.nih.gov/pmc/articles/PMC1179953/pdf/jphysiol00438-0625.pdf

[26] I. D. Loram, C. N. Maganaris, and M. Lakie, "Use of ultrasound to make noninvasive in vivo measurement of continuous changes in human muscle contractile length," *Journal of applied physiology*, pp. 1311–1323, 2006. [Online]. Available: http://www.jappl.org/content/100/4/1311.short

[27] N. J. Cronin, C. P. Carty, R. S. Barrett, and G. Lichtwark, "Automatic tracking of medial gastrocnemius fascicle length during human locomotion," *Journal of Applied Physiology*, vol. 111, no. 5, pp. 1491–1496, 2011. [Online]. Available: http://jap.physiology.org/content/111/5/1491

[28] D. J. Farris and G. A. Lichtwark, "UltraTrack: Software for semi-automated tracking of muscle fascicles in sequences of B-mode ultrasound images," *Computer Methods and Programs in Biomedicine*, vol. 128, pp. 111–118, 2016. [Online]. Available: http://dx.doi.org/10.1016/j.cmpb.2016.02.016

[29] N. J. Cronin, T. Rantalainen, and J. Avela, "Triceps surae fascicle stretch is poorly correlated with short latency stretch reflex size," *Muscle and Nerve*, 2015.

[30] M. Ishikawa and P. V. Komi, "The role of the stretch reflex in the gastrocnemius muscle during human locomotion at various speeds," *Journal of Applied Physiology*, vol. 103, no. 3, pp. 1030–1036, 2007.

[31] T. Deffieux, J.-L. Gennisson, M. Tanter, and M. Fink, "Assessment of the mechanical properties of the musculoskeletal system using 2-D and 3-D very high frame rate ultrasound." *IEEE transactions on ultrasonics, ferroelectrics, and frequency control*, vol. 55, no. 10, pp. 2177–2190, 2008.

[32] M. Tanter and M. Fink, "Ultrafast imaging in biomedical ultrasound," *IEEE Transactions on Ultrasonics, Ferroelectrics, and Frequency Control*, vol. 61, no. 1, pp. 102–119, 2014.

[33] B. Bolsterlee, S. C. Gandevia, and R. D. Herbert, "Ultrasound imaging of the human medial gastrocnemius muscle: How to orient the transducer so that muscle fascicles lie in the image plane," *Journal of Biomechanics*, vol. 49, no. 7, pp. 1002–1008, 2016. [Online]. Available: http://dx.doi.org/10.1016/j.jbiomech.2016.02.014

[34] T. Deffieux, J. L. Gennisson, M. Tanter, M. Fink, and A. Nordez, "Ultrafast imaging of in vivo muscle contraction using ultrasound," *Applied Physics Letters*, vol. 89, no. 18, 2006.

[35] J. Darby, E. F. Hodson-Tole, N. Costen, and I. D. Loram, "Automated regional analysis of B-mode ultrasound images of skeletal muscle movement." *Journal of Applied Physiology*, vol. 112, no. 2, pp. 313–327, 2012. [Online]. Available: http://jap.physiology.org/content/early/2011/10/25/japplphysiol.00701.2011.abstract{\%}5Cnhttp://www.ncbi.nlm.nih.gov/pubmed/22033532

[36] D. Miguez, I. Loram, and P. J. Harding, "A technical note on variable inter-frame interval as a cause of non-physiological experimental arte-

facts in ultrasound Subject Category : Subject Areas :," *R Soc open sci*, vol. 4, 2017.

APPENDIX A
EXPERIMENTAL CONSIDERATIONS FOR USING ULTRASOUND WITH SYSTEM IDENTIFICATION

A. 1) The frame rate of the ultrasound system

A first limitation lies in the frame rate that can be achieved. If it is desired to see the full fascicle when imaging then a large ultrasound probe is necessary. Usually probes of 50-60mm are used. A wider probe means that more ultrasound lines are necessary to build up the image. To see both SOL and GM muscle imaging up to a depth of 6cm is necessary. For a system that uses conventional line-by line imaging these factors limited the achievable frame rate. For example with the Philiphs HD7 system that was used initially for this study the maximum achievable frame rate was 42Hz with a probe of 50mm imaging at a depth of 6 cm. For other imaging systems that use line-by-line imaging this limit will be roughly the same, since the duration is largely limited by the speed of sound and only a marginally affected by the processing time. This limits the time resolution and consequently the frequencies that can be included in the continuous perturbation signal. Some systems can skip image lines, but this is negatively affects the spatial resolution. Higher frame rates have been shown to be achievable with ultrasound equipment that uses multi-line imaging.

B. 2) The number of consecutive frames the apparatus can record

A second consideration is the capability that the ultrasound system has for synchronization with other signals. Some ultrasound system are capable of producing a TTL signal at the start of the ultrasound recording or can use an external input to trigger the start of ultrasound recordings, while others don't have either capability. Besides a known start time, it is also important to know the precise recording time of each ultrasound frame. Miguez [36] showed that the inter-frame-interval (IFI) is not always constant for all systems. For the Philips HD7 machine the IFI could be read out and was shown to be very consistent. It thus depends on the machine if this is a concern and consequently if the IFI needs to be recorded.

C. 3) Synchronization of the ultrasound recording with the other measurements that are recorded

The third consideration is the recording duration, which is especially important for continuous perturbations. For example the Philips HD 7 system was limited to recording 360 frames consecutively, which at a frame rate of 42Hz meant a maximum recording duration of 8.6 seconds. An attempted solution to this was to use a videocard to capture the screen output instead of using the ultrasound to save the images. This method allows longer recordings. Also, relatively inexpensive videocards have the capability of recording frames at 50Hz. It would thus seem possible to make recordings up to that frame rate, but the videocard recordings still have to be synchronized with the rest of the signals. To try to achieve this use was made of the systems capabilities to synchronize ultrasound recordings with an electrocardiogram (ECG). Where normally a recorded ECG signal was displayed on screen alongside with the ultrasound images a start and stop signal was now displayed on command of the ankle robot. This enabled locating the first and last frame. Unfortunately, this solution was not viable for two reasons. Firstly, the displayed start-stop signal was only displayed with a resolution of 30Hz, which lead to imprecise start-stop timing. Secondly, the ultrasound images were updated in segments and not replaced as a whole. As a result the videocard recordings consisted of a compositions of two frames. Consequently, the motion is not accurately represented at the intended time resolution.

APPENDIX B
THE ADMITTANCES AND COHERENCES OF INDIVIDUAL PARTICIPANTS

The admittance of the contact torque with respect to the pedal angle, the admittance of joint torque with respect to GM length and the admittance of the joint torque with respect to SOL length are visualized for both the active and reflex task for all participants in Figures 18,19,20 and 21. These figures also show the higher the coherences for the ankle angle during the relax task for all participants.

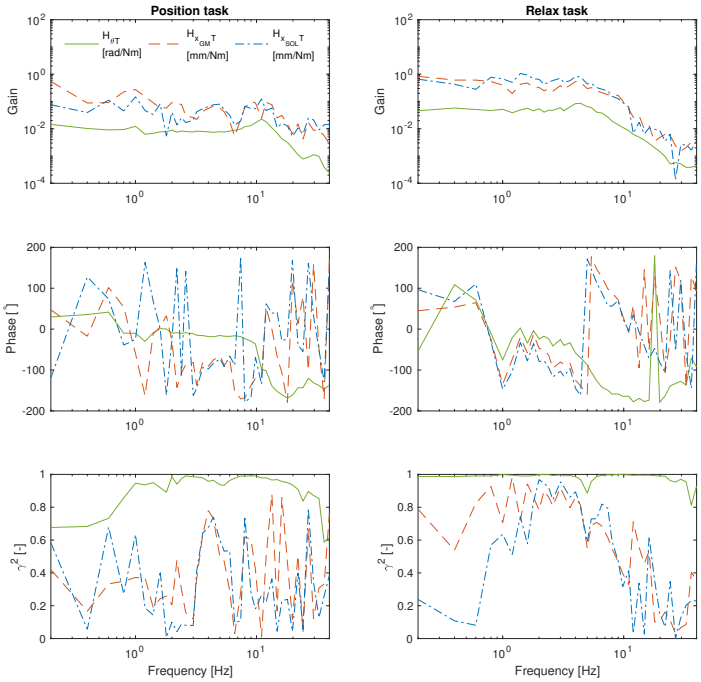

Fig. 18: Participant 5.

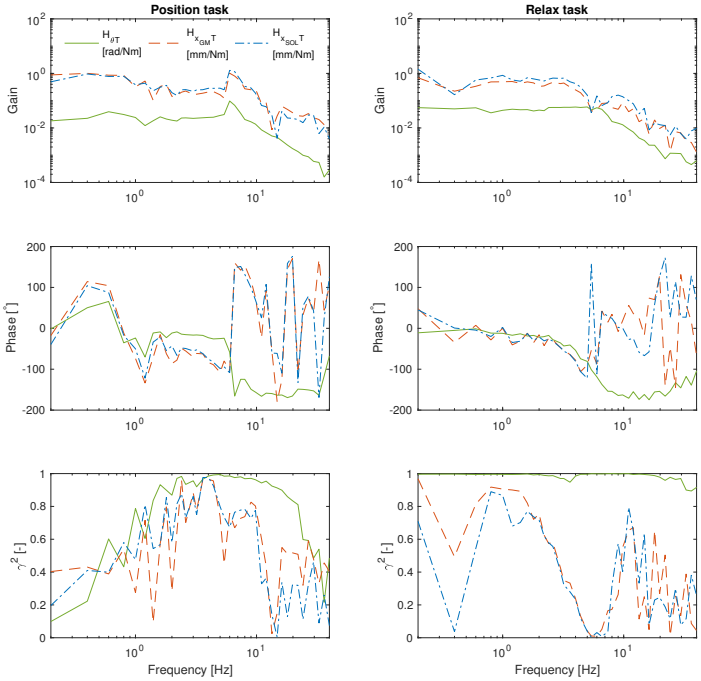

Fig. 19: Participant 6.

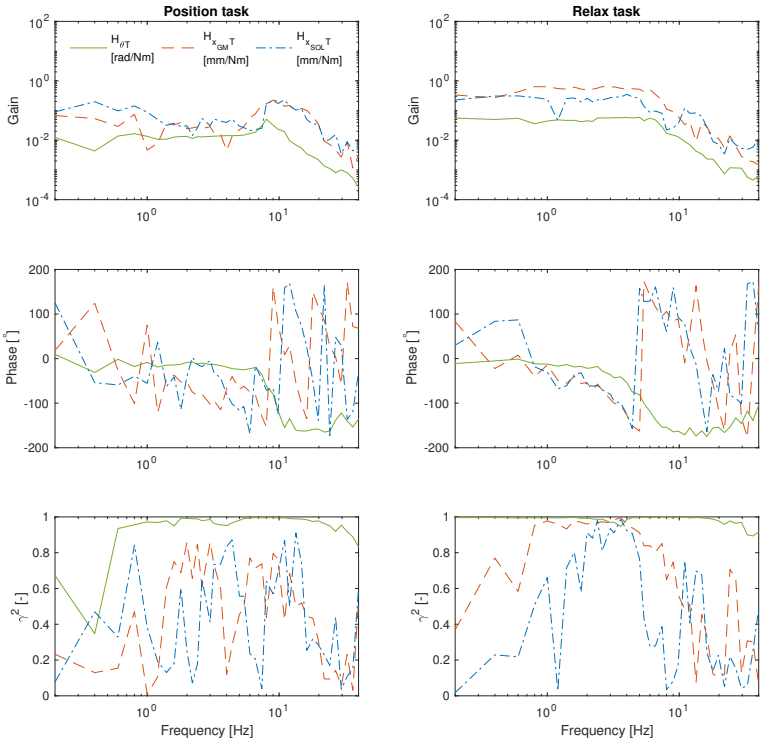

Fig. 20: Participant 7.

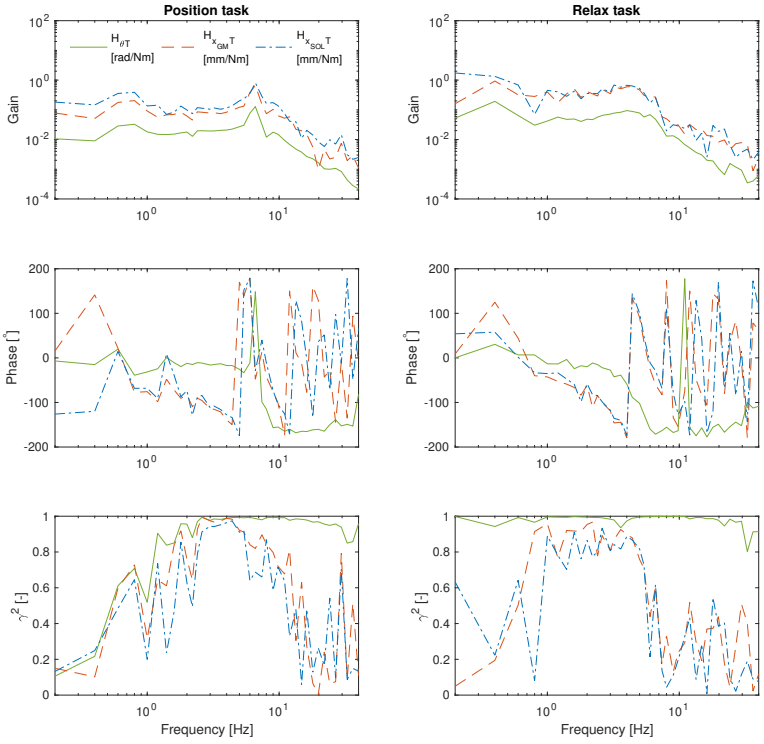

Fig. 21: Participant 8.

APPENDIX C
DATA OF ALL PARTICIPANTS DURING EXPERIMENT 2

It can be seen that the muscle stretch response to the RaHs is very consistent for a single participant, however the response differs between participants in the amount of oscillation. This is true, both for the active task in Figures 22, 23, 24, 25 and the passive task in Figures 26, 27, 28, 29.

A. Active

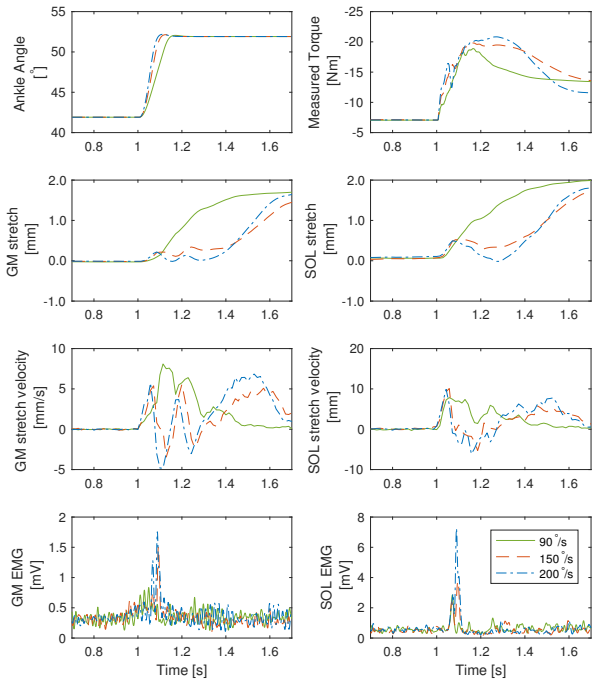

Fig. 22: Participant 1

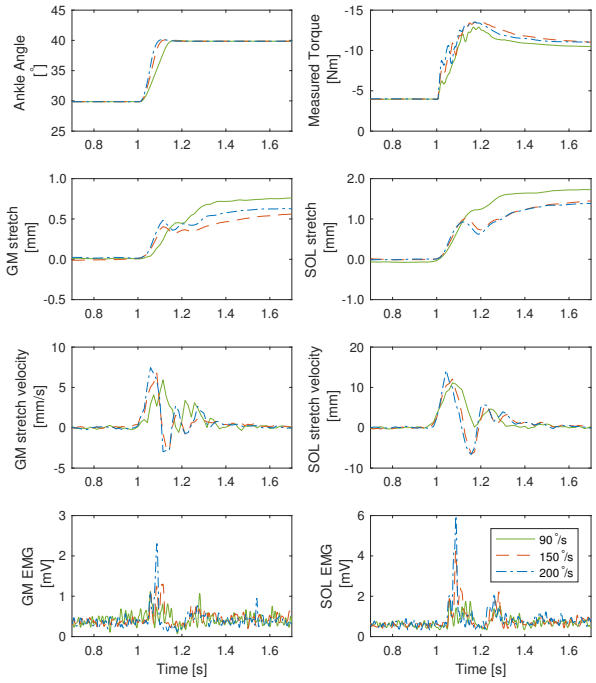

Fig. 23: Participant 2

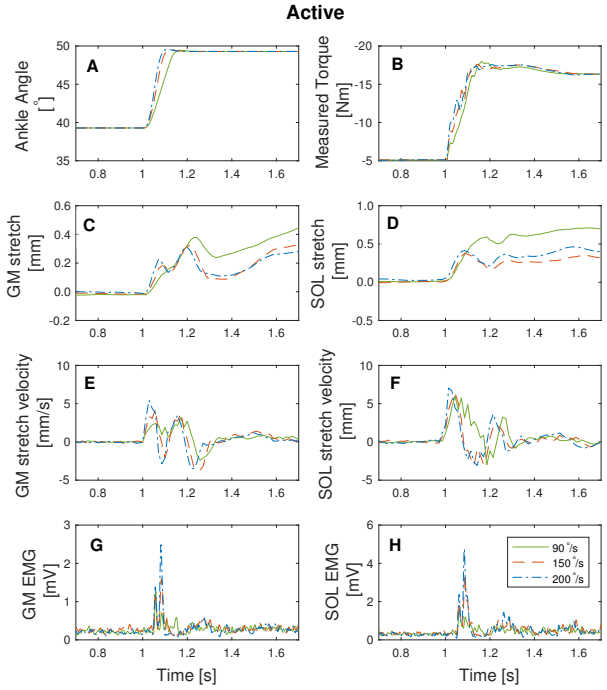

Fig. 24: Participant 3

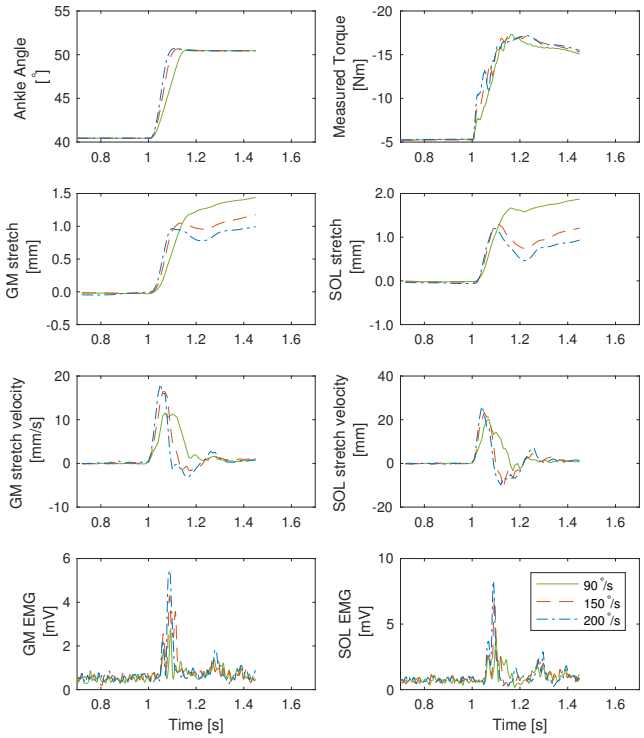

Fig. 25: Participant 4

B. Passive

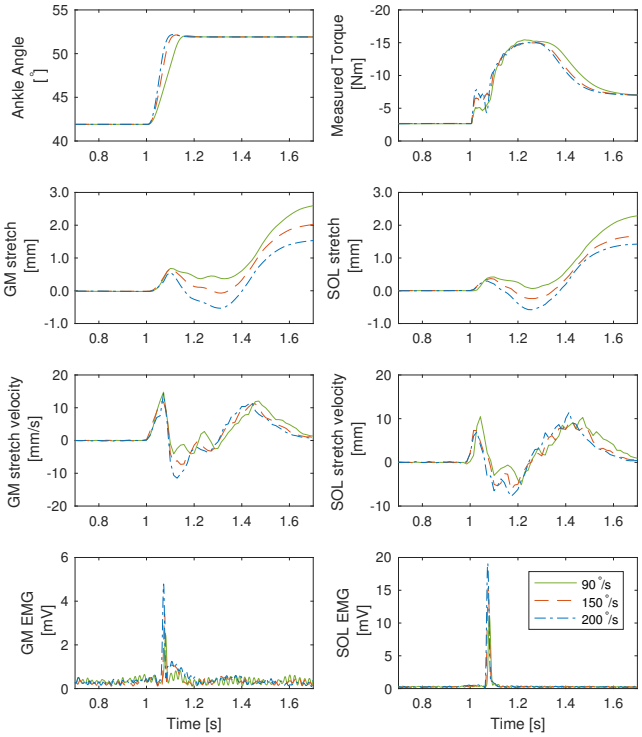

Fig. 26: Participant 1

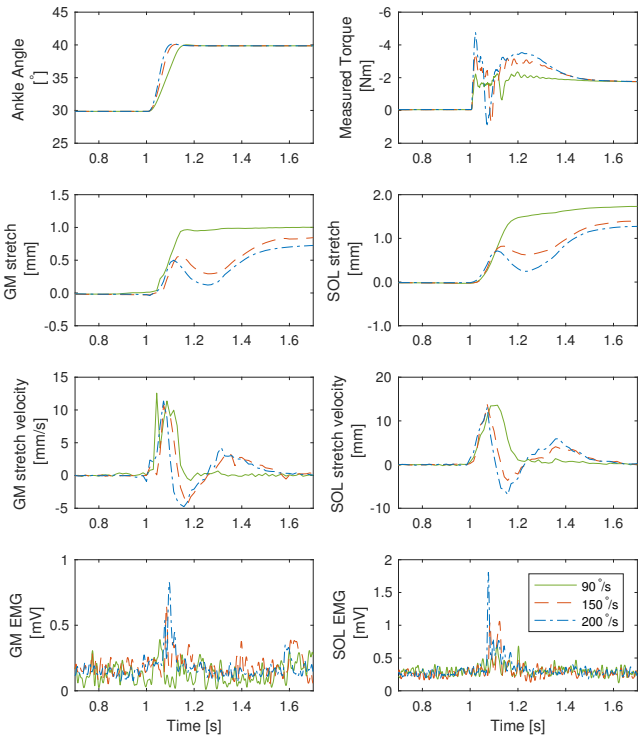

Fig. 27: Participant 2

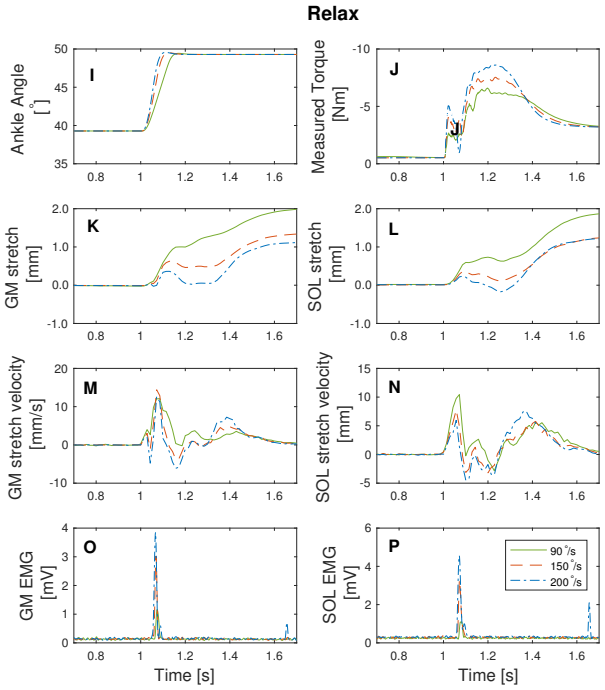

Fig. 28: Participant 3

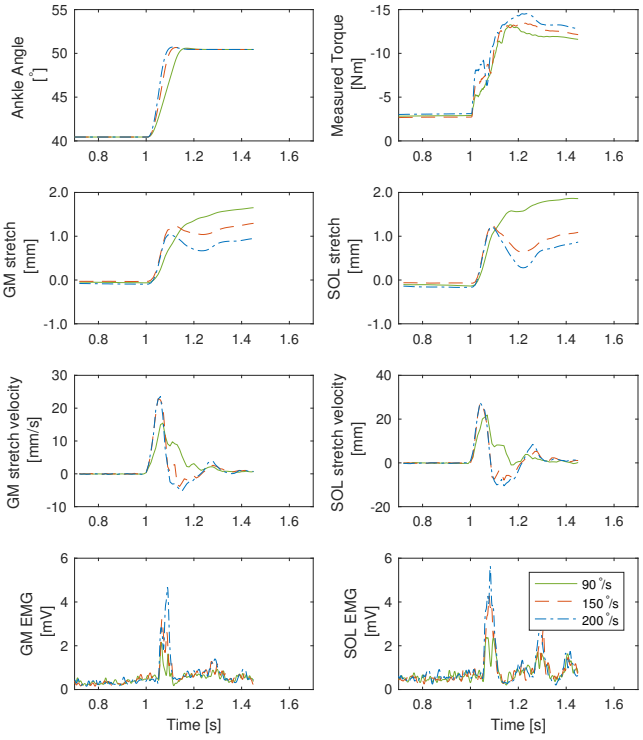

Fig. 29: Participant 4

APPENDIX D
INDIVIDUAL TRACKS OF RAH

This appendix shows the individually recorded responses of the GM and SOL muscle to the RaH perturbations for one subject during the active task. Responses that satisfied one or more of the criteria for exclusion as described in the Method section, were not included. Response to 90°/s disturbances for the GM and SOL can be seen in Figure 30 and 31. Responses to the 150 °/s perturbation in Figures 32 and 33 and responses to the 200 °/s perturbation in Figures 34 and 35.

A. Subject 1

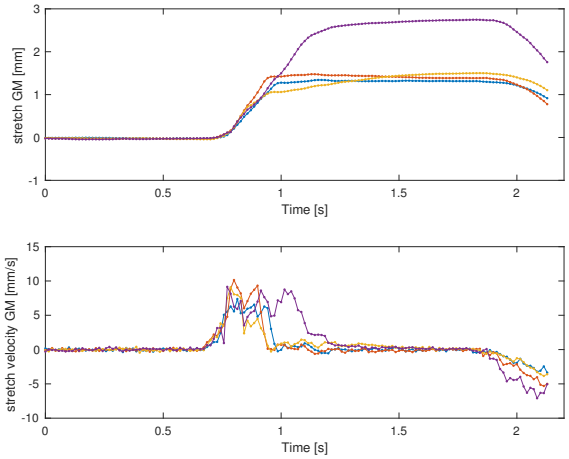

Fig. 30: Participant 1: response of the GM to disturbances of 90°/s. Trials remaining after exclusion are shown.

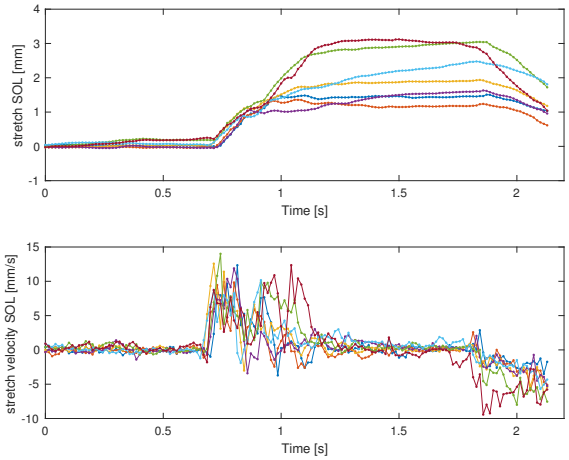

Fig. 31: Participant 1: response of the SOL to disturbances of 90°/s. Trials remaining after exclusion are shown.

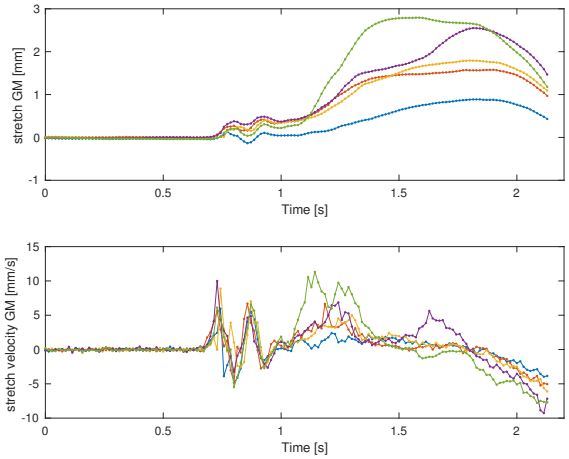

Fig. 32: Participant 1: response of the GM to disturbances of 150°/s. Trials remaining after exclusion are shown.

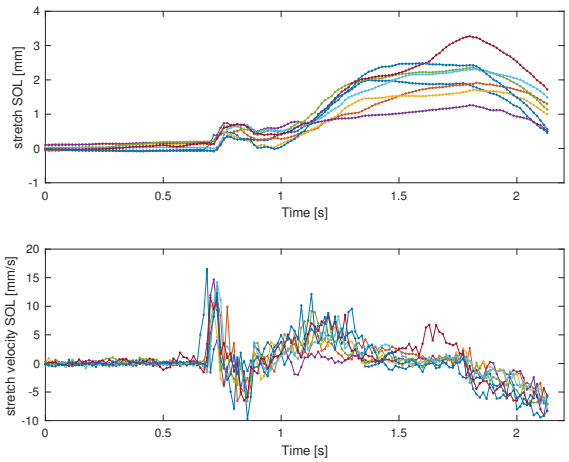

Fig. 33: Participant 1: response of the SOL to disturbances of 150°/s. Trials remaining after exclusion are shown.

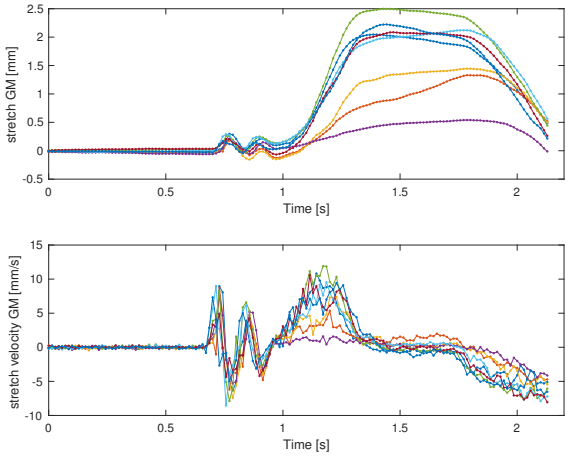

Fig. 34: Participant 1: response of the GM to disturbances of 200°/s. Trials remaining after exclusion are shown.

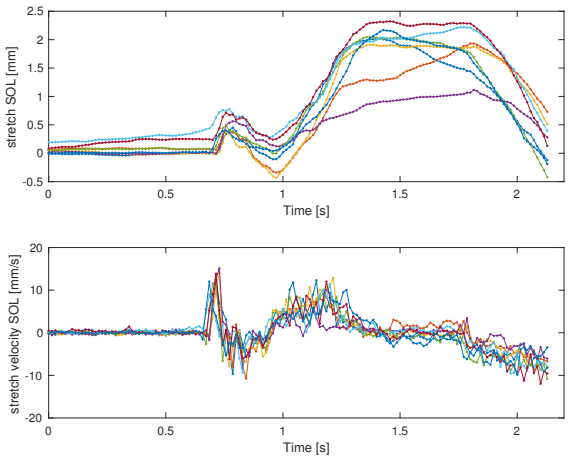

Fig. 35: Participant 1: response of the GM to disturbances of 200°/s. Trials remaining after exclusion are shown.

APPENDIX E
ADMITTANCE BETWEEN ANKLE ANGLE AND MUSCLE LENGTH FROM ALL RECORDED SEGMENTS.

Without detrending or excluding recorded segments the frequency response function between ankle angle and muscle length and the coherence of muscle length were as seen in Figures 36 and 37.

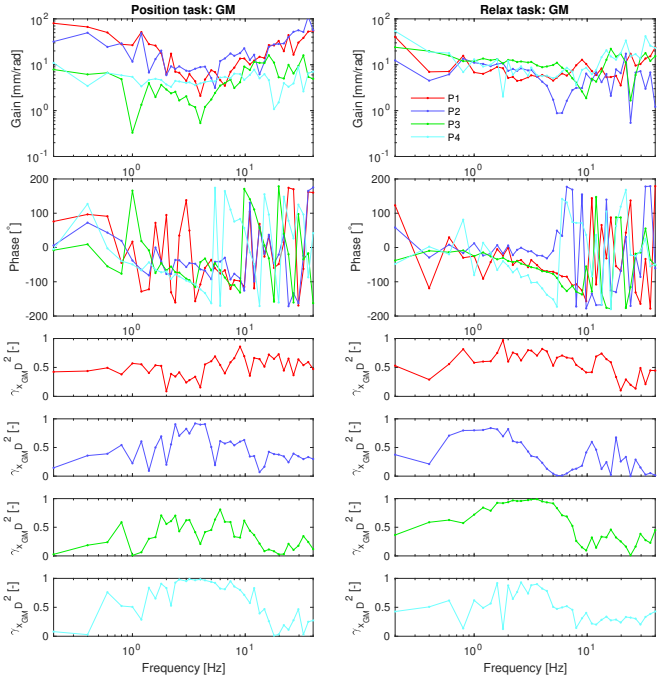

Fig. 36: GM

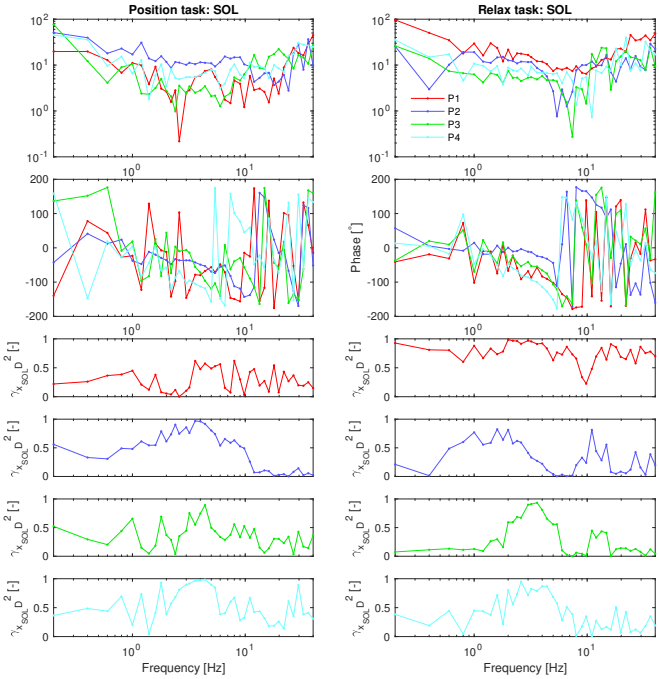

Fig. 37: Soleus